

The SBF Survey of Galaxy Distances. IV. SBF Magnitudes, Colors, and Distances¹

John L. Tonry²

Institute for Astronomy, University of Hawaii, Honolulu, HI 96822

Electronic mail: jt@ifh.hawaii.edu

Alan Dressler

Carnegie Observatories, 813 Santa Barbara St., Pasadena, CA 91101

John P. Blakeslee³

Dept. of Physics, University of Durham, South Road, Durham, DH1 3LE, United Kingdom

Edward A. Ajhar²

Kitt Peak National Observatory, National Optical Astronomy Observatories, P. O. Box 26732,

Tucson, AZ 85726

André B. Fletcher

MIT Haystack Observatory, Off Route 40, Westford, MA 01886

Gerard A. Luppino

Institute for Astronomy, University of Hawaii, Honolulu, HI 96822

Mark R. Metzger

Caltech Astronomy Dept, MS 105-24, Pasadena, CA 91125

Christopher B. Moore

Harvard-Smithsonian Center for Astrophysics, 60 Garden St., Cambridge, MA 02140

¹Observations in part from the Michigan-Dartmouth-MIT (MDM) Observatory.

²Guest observers at the Cerro Tololo Inter-American Observatory and the Kitt Peak National Observatory, National Optical Astronomy Observatories, which are operated by AURA, Inc., under cooperative agreement with the National Science Foundation.

³Current address: Department of Physics and Astronomy, Johns Hopkins University, Baltimore, MD 21218

ABSTRACT

We report data for I band Surface Brightness Fluctuation (SBF) magnitudes, $(V-I)$ colors, and distance moduli for 300 galaxies. The Survey contains E, S0 and early-type spiral galaxies in the proportions of 49:42:9, and is essentially complete for E galaxies to Hubble velocities of 2000 km s^{-1} , with a substantial sampling of E galaxies out to 4000 km s^{-1} . The median error in distance modulus is 0.22 mag.

We also present two new results from the Survey. (1) We compare the mean peculiar flow velocity (bulk flow) implied by our distances with predictions of typical cold dark matter transfer functions as a function of scale, and find very good agreement with cold, dark matter cosmologies if the transfer function scale parameter Γ , and the power spectrum normalization σ_8 are related by $\sigma_8 \Gamma^{-0.5} \approx 2 \pm 0.5$. Derived directly from velocities, this result is independent of the distribution of galaxies or models for biasing. The modest bulk flow contradicts reports of large-scale, large-amplitude flows in the $\sim 200 \text{ Mpc}$ diameter volume surrounding our Survey volume. (2) We present a distance-independent measure of absolute galaxy luminosity, \overline{N} , and show how it correlates with galaxy properties such as color and velocity dispersion, demonstrating its utility for measuring galaxy distances through large and unknown extinction.

Subject headings: galaxies: distances and redshifts — galaxies: clusters: individual (Virgo, Centaurus) — cosmology: distance scale — cosmology: large-scale structure of universe

1. Introduction: A Brief History of SBF

The *I*-band Surface Brightness Fluctuation (SBF) Survey was undertaken to measure accurate distances to nearby galaxies in the expectation of tying Cepheid distances to the far-field Hubble flow and substantially improving our knowledge of the local velocity field. The Survey was inaugurated with the work of Tonry, Ajhar, & Luppino (1990), who measured *VRI* SBF magnitudes with the Kitt Peak 4m telescope for 14 early-type galaxies, mostly members of the Virgo cluster. Tonry (1991) followed with the first fully empirical, though provisional, calibration of the method, based on the Cepheid distance to M31 and the color dependence of the *I*-band SBF magnitude \overline{m}_I for Fornax cluster galaxies observed with the 4m telescope at Cerro Tololo. The data collection has spanned a decade now, with most of the recent northern data coming from the MDM 2.4m on Kitt Peak and the southern data coming from the Las Campanas 2.5m. A recent review of SBF can be found in Blakeslee, Ajhar, & Tonry (1999).

The present series of papers began with Tonry et al. (1997, hereafter SBF-I), which detailed how the SBF survey data from different telescopes and observing runs were intercompared and brought into a homogeneous system, and how error estimates were derived. In SBF-I, a new *I*-band calibration with a significantly different zero point was presented, and various methods were used to tie to the far-field Hubble flow in order to derive the Hubble constant. Tonry et al. (2000, SBF-II) used the SBF survey data to construct a parametric flow model which included infall into the Virgo and the Great Attractors, a residual quadrupole, an overall dipole (bulk flow of the sample), the cosmic thermal velocity dispersion, and the Hubble constant, all as free parameters. SBF-II also revised the zero point by using the latest Cepheid distances tabulated by Ferrarese et al. (2000) and the new DIRBE/IRAS Galactic extinction estimates from

Schlegel, Finkbeiner, & Davis (1998). Blakeslee et al. (1999, SBF-III) used the same data set to compare the measured SBF peculiar velocities to predictions that derived from the galaxy density field measured by flux-limited redshift surveys, under the assumption that light traces mass with a linear biasing prescription. This comparison yielded values for both the Hubble constant and $\beta \equiv \Omega^{0.6}/b$, where Ω is the matter density and b is the linear bias of the observed galaxies.

In addition to the *I*-band ground-based survey, there have been a number of recent SBF efforts in the F814W filter of WFPC2 on the Hubble Space Telescope (HST). Ajhar et al. (1997) gave the initial calibration of the method for this filter. Lauer et al. (1998) measured SBF distances to four brightest cluster ellipticals at distances of $\sim 5000 \text{ km s}^{-1}$, and Pahre et al. (1999) measured the distance to NGC 4373 in the Hydra-Centaurus supercluster.

Recently, SBF measurements in near-infrared bandpasses have been added. Jensen, Luppino, & Tonry (1998a, 1998b) measured *K*-band SBF distances to galaxies in the Virgo, Fornax, Eridanus, Centaurus, and Coma clusters. Another HST study (Jensen et al. 2000, in preparation) calibrates the F160W near-infrared NICMOS filter for use with SBF and samples the Hubble flow out to $10,000 \text{ km s}^{-1}$. The use of SBF in stellar population synthesis has received renewed interest of late (e.g. Liu, Charlot, & Graham 2000; Blakeslee, Vazdekis, & Ajhar 2000), both as a means for probing stellar populations and as an independent check of the Cepheid distance scale. These efforts underscore the importance of a solid empirical calibration of the method.

In this paper, we present and discuss the data from our *I*-band SBF distance survey and present two new results based on these data.

2. The Galaxy Sample

Because it was our intent to make this survey as homogeneous as possible our observations

span the entire sky, except for incomplete sampling of the zone of avoidance. It is difficult to make a really quantitative statement of our selection function, because SBF observability depends strongly on the atmospheric seeing, and we were quite limited by the availability of telescope time at the many facilities that were used to conduct this study. However, as a guide, we can compare with the RC3: Figure 1 shows how the cumulative counts rise with redshift in the SBF sample and the RC3. These are counts of galaxies with $B_T \leq 12.5$, which includes about 63% of the galaxies in the SBF survey. We are nearly complete in E galaxies to a Hubble velocity of 2000 km s^{-1} and have sampled a very substantial fraction even to 4000 km s^{-1} . The higher incompleteness for S0's compared to E's reflects both the added difficulty of adequate modeling of disk + bulge for some S0 galaxies and the fact that we chose not to observe many of the S0's in groups where we already had distances to elliptical galaxies. We have succeeded in measuring SBF magnitudes in only a few spiral galaxies, mostly ones with large, smooth bulges, and they are mostly at nearby distances where Cepheid observations are possible.

Figure 2 displays the distribution of galaxies in reddening-corrected $(V-I)$ color. The colors used here (those in Table 1) are derived from the regions of the galaxies in which the SBF analyses were performed. Overall, the mean color is $\langle V-I \rangle_0 = 1.145$ and the rms dispersion is 0.06 mag. The ellipticals follow a more or less Gaussian color distribution centered at $(V-I)_0 = 1.165$ with a dispersion of only 0.04 mag. The blue tail extending to $(V-I) < 1.0$ is comprised mainly of S0 galaxies.

3. Calibration Issues

We described in SBF-I how we brought all of the photometry onto a common system and how we validated our error estimates for $(V-I)$ and \bar{m}_I through multiple observations. Groups of galaxies were used to establish the slope of the

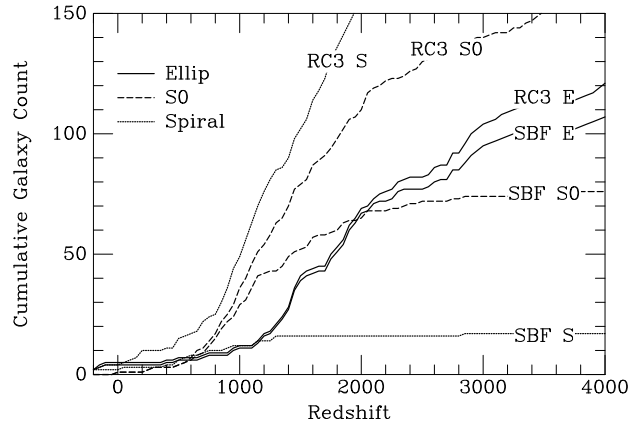


Fig. 1.— The cumulative counts of galaxies with $B_T \leq 12.5$ are shown for the RC3 (upper curves) and the SBF survey (lower curves). The three sets of curves show counts of E, S0, and Sa and Sb spiral galaxies with $T \leq 3$.

$\bar{m}_I(V-I)$ relationship, and we compared the relative group distances with those from other distance estimators to demonstrate the apparent universality of the $\bar{m}_I(V-I)$ relationship. By comparison with the extant Cepheid distances we also chose a zero point for the $\bar{M}_I(V-I)$ relation and reported that the relations for ellipticals, S0 galaxies and spiral bulges are indistinguishable with the present data.

In SBF-II, we described our switch from the older Burstein & Heiles (1984) H I-derived extinction estimates to the new Schlegel, Finkbeiner, & Davis (1998, hereafter SFD) extinctions based on the DIRBE/IRAS maps. The SFD values are preferable because of their greater homogeneity over the sky and greater angular resolution, and they are probably more accurate (see SFD). The change affects our reductions of both \bar{m}_I and $(V-I)$ to extinction-free values. Despite an overall shift in $E(B-V)$ of nearly 0.02 mag, there was little change to the distance estimates for most galaxies because our zero point also comes from galaxies with revised extinction estimates. Nevertheless, these values for \bar{m}_I and $(V-I)$ should *not* be mixed with previously published

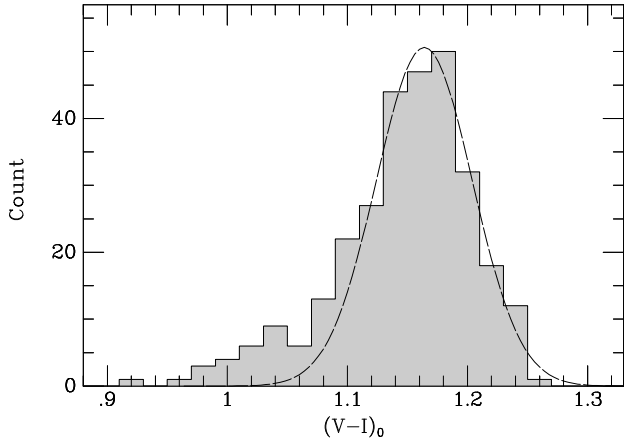


Fig. 2.— The $(V-I)$ distribution of SBF survey galaxies, represented by the shaded histogram. The dashed curve shows for comparison a Gaussian of mean $(V-I) = 1.16$ and dispersion 0.04 mag.

data without due attention to the differing assumptions about extinction.

The zero point for the $\overline{M}_I-(V-I)$ relation continues to be a work in progress, unfortunately, as we discuss in detail in SBF-II. While there is concurrence that the slope of the $\overline{M}_I-(V-I)$ relation derived in SBF-I is accurate, uncertainty in the zero point remains at the 0.1 mag level. Essentially, the SBF zero point can be calibrated using Cepheid distances or theory. The Cepheid distances can be applied to SBF measurements either galaxy by galaxy or through group association of galaxies with Cepheid distances to other galaxies with SBF distances. SBF-II adopted the former approach and derived

$$\overline{M}_I = -1.74 \pm 0.08 + (4.5 \pm 0.25)[(V-I)_0 - 1.15] \quad (1)$$

using the HST Key Project Cepheid distances (Ferrarese et al. 2000). The validity of this equation has been tested for colors in the range of $0.95 < (V-I)_0 < 1.30$. Our zero point is based on the median value for six spirals with both Cepheid and SBF measurements; using a similar approach and a weighted average, Ferrarese

et al. (2000) derived a zero point of -1.79 ± 0.09 .

The uncertainty in the SBF zero-point is illustrated by comparing these values to the result of the group-association method. As we discuss in SBF-II, using a group association between Cepheid-bearing spirals and early-type galaxies with SBF measurements results in a significant change in the zero point to -1.61 ± 0.03 . The fainter group-based calibration points to either systematically brighter SBF magnitudes for spiral bulges or, as found by Kelson et al. (2000) in the context of the fundamental plane calibration, a systematic offset for the Key Project spirals to lie in front of the ellipticals in the same groups. Additional data will be needed to resolve the cause of this discrepancy and thereby firm up the SBF calibration.

We emphasize that the error bars given here do *not* include the systematic uncertainty in the Cepheid zero point, estimated by Mould et al. (2000) to be ± 0.16 mag, which allows for ± 0.13 mag of uncertainty in the adopted LMC distance modulus of 18.50 mag. This uncertainty should be taken seriously, since the distance to the LMC remains controversial. At the time of this writing, Freedman et al. (2000) are preparing a major revision in the Cepheid distance scale based on a reassessment of the LMC distance from seven independent means, an improved PL relation based on the new, large sample of LMC Cepheids from the OGLE Project, and a small metallicity dependence for the PL relation. Application of these new Cepheid distances to our six calibrating galaxies will make our SBF calibration fainter by ~ 0.1 mag with a corresponding rise in the Hubble constant of about 5%.

A final example of the continuing uncertainty in the SBF calibration comes from its derivation purely from stellar evolution theory and population synthesis. Worthey (1993a, 1993b, 1994) was the first to accurately reproduce the empirical slope of the $\overline{M}_I-(V-I)$ relation; these models gave a theoretical zero point of -1.81 (see SBF-I), consistent with the value in eq. (1)

from the Cepheid calibration. Liu et al. (2000) use an updated version of the Bruzual & Charlot (1993) models with the isochrones of Bertelli et al. (1994) and find a similar I -band zero point value of -1.79 . These authors revised the AGB evolution in their models because the original Bruzual & Charlot AGB prescription gave a \overline{M}_I zero point significantly fainter than the empirical result. The uncertainty in modeling the AGB is a lingering problem for the theoretical derivation of the I -band zero point and will be an even bigger problem for the K band. Indeed, a fully independent re-derivation by Blakeslee et al. (2000) using new models based on the latest isochrones from the Padua group (Girardi et al. 2000) and empirical color-temperature transformations has yielded a value that is significantly different. They reproduce the observed fluctuation colors well and also match the empirical I -band slope, but find a zero point of -1.47 , i.e., 0.27 mag brighter than in eq. (1). The discrepancy drops to 0.14 mag for the SBF-II group calibration, and then would essentially disappear for the revised Key Project Cepheid scale referred to above. As Blakeslee et al. discuss, the theoretical uncertainty also reflects a moderate sensitivity to the uncertain details of stellar evolution, for example, the distribution and lifetimes of stars on the red giant branch.

Although we look forward to advances in stellar evolution theory that will allow a robust theoretical SBF zero point, this is not likely to happen soon. For now, the empirical zero point appears more reliable.

4. The Data

Table 1 presents colors, fluctuation magnitudes, and distance moduli of the galaxies in the SBF sample. The columns are (1) galaxy name; (2) right ascension (J2000) from the RC3; (3) declination (J2000); (4) redshift (km s^{-1} , CMB reference frame); (5) morphological T type; (6) group number as defined by the Faber et al. (1989 7S); (7) B band extinction adopted from

SFD; (8) $(V-I)$ color measured at radii indicated in column 11, error, and number of contributing measurements; (9) I band fluctuation magnitude, error, and number of contributing measurements; (10) distance modulus using eq. (1) for \overline{M}_I as a function of $(V-I)$, including all sources of error except systematic error in the zero point; (11) mean annular radius (arcsec) contributing to the SBF measurement, ratio of the innermost contributing radius to the mean, and ratio of the outermost contributing radius to the mean; (12) observation quality, as defined in SBF-II: $Q = \log_2[N_e(\overline{m})/\text{PD}^2]$, where $N_e(\overline{m})$ is the number of electrons that would be detected in the image from an object of magnitude \overline{m} , and PD is the product of the full-width at half-maximum of the point spread function (PSF) in arcseconds and the CMB frame velocity in units of 1000 km s^{-1} (so PD^2 is proportional to the metric area within a resolution element); (13) “PD” value defined above; and (14) \overline{N}_I , discussed below. Note that the seeing (in arcseconds) of the observation can be derived as PD divided by the CMB velocity in units of 1000 km s^{-1} , except that galaxies within 3° of NGC 4486 and with heliocentric velocity less than 2400 km s^{-1} were assigned a PD velocity of 1350 km s^{-1} , galaxies within 2° of NGC 4709 and with heliocentric velocity between 3800 and 4800 km s^{-1} were assigned a PD velocity of 3100 km s^{-1} , and other galaxies with a negative redshift were assigned a velocity of 10 km s^{-1} .

Table 2 adds a few galaxies whose distances are potentially biased either because the seeing was poor for the distance ($\text{PD} > 2.7$) or the quality was poor ($Q < 0$). These observations were deemed unacceptable for use in SBF-II, but we include them here despite the potential for bias they do provide at least crude distances and because the photometry is good. (The data of Table 2 might also be useful to further study of the degree of bias present in this data set.) We also include NGC 3413 in this table because it is a very dusty galaxy and its color is significantly bluer

than our empirical calibration allows. NGC 4627 has likewise been relegated to this table for being too blue. We still lack adequate photometry to provide colors for NGC 1331, NGC 3522, and IC 5269. The columns in this table are the same as with Table 1. We stress that these data should be used with caution and should not be mixed with the observations from Table 1.

Tables 1 and 2 are available in digital form from <http://www.ifa.hawaii.edu/~jt/SBF> in table.good and table.poor.

Table 3 gives values for \overline{m} in different bandpasses. The columns are mostly self explanatory, but the second column lists the mean radius (in arcsec) where the fluctuation magnitudes and colors were measured in NGC 205. These data come from a single observing run (M0893; see SBF-I for details), and although they are subjected to the same calibration as the other data, some of the \overline{m}_I will not be identical to Table 1. We hope, however, that the internal consistency of these data will be better than by using the average \overline{m}_I from Table 1 and therefore the fluctuation colors will be more accurate. Note that these data make it obvious that NGC 404 is not a member of the Local Group, but lies at a distance of about 3 Mpc.

Table 4 gives “group average” distances for the galaxy defined in SBF-I. In particular, the membership criteria are based on position on the sky and redshift, not necessarily the group assignment made by the 7S, although we give the group number defined by the 7S that most closely corresponds to the SBF groups. The distance errors do not take any account of the extent of the group, hence are probably unrealistically small. It would now probably be appropriate to select the groups with some knowledge of the SBF distances (this would have been circular in SBF-I); what we present here is only meant as a rough guide to group properties. More precise group distances can be derived from better group definitions and from Table 1.

5. The Local Velocity Field

Using the data just presented, we made a first effort to extract the peculiar velocities in SBF-II (where we fit a parametrized model) and SBF-III (where we match the flow field inferred from IRAS galaxy counts). The important results from those papers are that we prefer the value for H_0 of 74 ± 4 from SBF-III (but dependent on the Cepheid zero point as described above). We find in SBF-III that $\beta_I = \Omega^{0.6}/b_I = 0.42$ for the IRAS 1.2 Jy survey (Fisher et al. 1995), and $\beta_O = 0.26$ for the “Optical Redshift Survey” (Santiago et al. 1995), which is consistent with $b_{IRAS} = 1$, $b_{opt} = 1.6$, and $\Omega_M = 0.25 \pm 0.05$.

Because of the interest over the last five years in even larger flows on very large scales (e.g., Lauer & Postman 1994; Hudson et al. 1999; Willick 1999), we wish to expand here on the result in SBF-II which contradicts these claims. Basically, the evidence is that, according to our SBF model, the major part of the CMB dipole is generated within a volume $V \lesssim 5000 \text{ km s}^{-1}$. This means that to accept the existence of these larger bulk flows in a volume that is much larger than this (but includes it) is to find that our subvolume is basically at rest with respect to the CMB while material around that volume is, on average moving with a high velocity ($\gtrsim 600 \text{ km s}^{-1}$). This situation implies an improbable, if not impossible, spectrum of initial fluctuations, very different from the scale-free power spectrum that underlies cold-dark-matter (CDM) models.

In contrast, our measure of the bulk flow as a function of scale within our SBF Survey volume is in good agreement with theoretical predictions of typical cold-dark-matter (CDM) models based on a scale-free power spectrum, as we now show. The “SBF-II model” gives us a smooth measure of mean velocity and velocity dispersion throughout the survey volume, which is valid within $|SGX|, |SGY| < 50 \text{ Mpc}$, and $|SGZ| < 25 \text{ Mpc}$. Figure 3 illustrates how well a

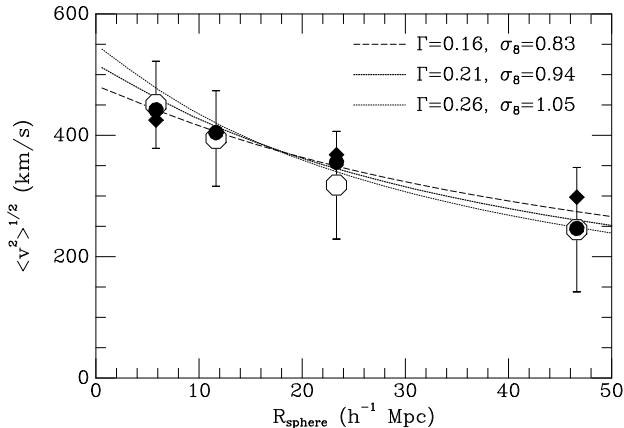


Fig. 3.— The bulk flow observed and predicted in top-hat spheres of radius R is shown for typical CDM models of the power spectrum (curves), a simulated universe with a $\Gamma = 0.21, \sigma_8 = 0.94$ CDM power spectrum (large open points), and for the SBF-II observations (circles for SBF-II model, diamonds for Willick and Batra variant). The simulated universe encompasses many volumes equal to that of the SBF-II survey, and the rms variation in bulk flow seen from volume to volume is shown as error bars on the open points. Note that the radius is expressed in terms of h^{-1} Mpc for consistency with what is normally found in the literature. The rollover in the data points at $R < 10h^{-1}$ Mpc is caused by the limited spatial resolution of the SBF-II model.

typical CDM power spectrum matches the mean bulk flows of these data.

The points are generated by computing the SBF-II model velocity with respect to the CMB, averaged over cubes of varying size. The RMS of all the cubes within the survey volume gives us a bulk flow on that scale. We assign an effective spherical radius to the cube size by matching the volume of the sphere to that of the cube. The rolloff in the bulk flow data points at $R < 10h^{-1}$ Mpc is inherent in the parametrized model.

Willick and Batra (2000) have recently reexamined the SBF survey data and compared the

peculiar velocities with those expected from the IRAS density distribution. In addition, they redetermined parameters for the SBF-II model, and the bulk flows from the Willick and Batra model are also shown in Figure 3 to give a sense of the uncertainty inherent in the interpolation of the SBF peculiar velocities by this parametric model.

For comparison we also plot curves showing the bulk flow expected from a typical CDM power spectrum, using the parametrization of Bardeen et al. (1986) of the CDM transfer function and a flat cosmology with $\Omega_M = 0.3, \Omega_\Lambda = 0.7$. These transfer functions require a spatial scale parameter $\Gamma \sim \Omega_M h$ and a normalization which is commonly supplied by σ_8 , the rms mass fluctuation between spherical volumes of radius $8h^{-1}$ Mpc. We find that typical shape parameters of $\Gamma = 0.16, 0.21$, and 0.26 , and corresponding normalizations of $\sigma_8 = 0.83, 0.94$, and 1.05 match these observations of bulk flows very well.

We find negligible difference whether we use a cube window function or a top-hat, with side and radius related as above. To demonstrate this we show in Figure 3 open points which come from a numerical simulation of a universe with the $\Gamma = 0.21$ and $\sigma_8 = 0.94$ CDM power spectrum and random phases. The bulk flows in this simulation were computed in disjoint cubes precisely in the same way as the data were treated (with the same assignment of top-hat radii). Since the simulated universe encompassed a volume which was 8192 times as large as the SBF survey volume, it was also possible to assess the cosmic variance in bulk flow expected when velocity is measured within the finite SBF survey volume. This RMS variation, represented by the error bars on the simulation points in Figure 3, demonstrates that it will not be easy to put stringent limits on the CDM transfer function shape parameter Γ or normalization σ_8 individually, but that the combination $\sigma_8 \Gamma^{-0.5}$ is fairly well constrained at $\sigma_8 \Gamma^{-0.5} \approx 2 \pm 0.5$. This combination comes from the constraint these data

place on the slope of the power spectrum between $k \sim 0.2h \text{ Mpc}^{-1}$, which contributes to σ_8 , and $k \sim 0.04h \text{ Mpc}^{-1}$ which contributes to bulk flows. The (one sigma) error bar is dominated by the cosmic variance expected in the rather small SBF survey volume. The value of this measurement, of course, is that it is directly sensitive to the mass fluctuations on scales of $50\text{-}200h^{-1} \text{ Mpc}$ without any recourse to galaxy distribution or bias models.

In summary, the data of the SBF Survey seem completely compatible with conventional models of the formation of large scale structure, in contrast to the implications of even larger scale flows that have been reported.

6. Distance Independent Absolute Luminosities: \overline{N}

Developing more accurate ways of measuring absolute luminosity for galaxies that is independent of distance is obviously important for a wide range of astronomical issues. SBF is another, we believe, major step in that program. In the course of this study we have investigated a further parameterization which is, in addition, independent of photometric calibration or extinction as well. This measure of the absolute luminosity comes from the ratio of the total apparent flux from the galaxy and the flux provided by the fluctuation signal. We express this in terms of magnitudes as the difference between the fluctuation magnitude and the total magnitude of the galaxy:

$$\overline{N} = \overline{m} - m_T. \quad (2)$$

We call \overline{N} the ‘‘fluctuation star count:’’ it amounts to $+2.5 \log_{10}$ of the total luminosity of the galaxy in units of the luminosity of a typical giant star.

We give values for \overline{N} in the last columns of Tables 1 and 2. The total magnitudes were derived from the SBF survey photometry. A program written by B. Barris fitted a modified Sersic model (i.e., $\exp(-r^{1/n})$) and a sky offset to the azimuthally averaged profile (after removal

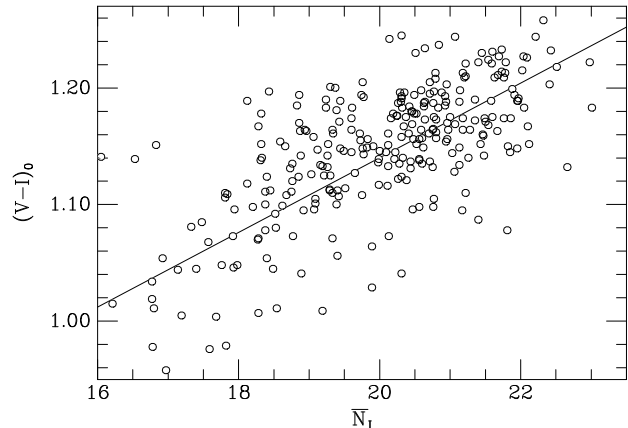


Fig. 4.— The $(V-I)$ color of SBF galaxies is shown as a function of \overline{N} .

of stars and companion galaxies). The extrapolation to infinity was converted to a total apparent magnitude. The difference between this total magnitude and the fluctuation magnitude yields \overline{N} . As is well known, this extrapolation can be quite uncertain because of the great extent of galaxies at low surface brightness; probably for this reason there are occasionally significant discrepancies between our total magnitudes in the I band and B_T values from the RC3 (which generally are derived forcing n to be 4). Therefore, we urge care in use of values of I_T recovered from the values we give for \overline{N} .

Not surprisingly, this absolute luminosity correlates with color; Figure 4 shows the dependence of $(V-I)$ on \overline{N} . This correlation is approximated by

$$(V-I) = 0.50 + 0.032\overline{N} \quad (3)$$

The slope of the relation is so shallow that a very large error in \overline{N} has negligible effect on the prediction of $(V-I)$ (a huge error of 0.5 mag in \overline{N} corresponds to an error of only 0.016 mag in $(V-I)$). The scatter in $(V-I)$ for all galaxies is approximately 0.04 mag. If we restrict ourselves to only bona-fide elliptical galaxies with the best measurements of \overline{m}_I (error less than 0.30 mag) and $(V-I)$ (error less than 0.02 mag), the scatter

decreases slightly to 0.03 mag. Inasmuch as the median error of the $(V-I)$ values used is 0.015 mag, this means that the intrinsic scatter in the prediction of $(V-I)$ from \overline{N} may be as small as 0.025 mag. This corresponds to an RMS uncertainty of only 0.02 mag in $E(B-V)$, which suggests that this is a promising way to measure extinctions.

For example, by measuring the I fluctuations in a galaxy which is hidden behind 3 mag of extinction, one could establish \overline{N} independent of the extinction, derive $(V-I)_0$ with an accuracy of 0.025 mag, \overline{M}_I with an uncertainty of 0.11 mag, A_I with an accuracy of 0.04 mag, and hence an SBF distance which has an error of only 0.12 mag from extinction. Although there is some covariance in the final answer from the use of \overline{m}_I for both the intrinsic color and the distance modulus, the slope of $(V-I)$ with \overline{N} is so shallow that the covariance is very mild.

The direct use of $(V-I)$ to estimate \overline{M}_I is operationally difficult both because of the sensitivity to dust extinction and also the necessity for very accurate photometry. Use of \overline{N} eases these requirements considerably.

In practice, this means that it is not necessary to go through $(V-I)$ at all to estimate the absolute \overline{M}_I , although some color information or estimate of dust extinction is eventually necessary to get a distance modulus. In order to demonstrate how \overline{M}_I depends on \overline{N} we must once again resort to groups so that \overline{m}_I differs from \overline{M}_I by only an offset. Figure 5 shows values for \overline{m}_I in eight groups as a function of \overline{N} . The lines are all drawn using the SBF distance modulus to the group based on the $(V-I)$ measure of \overline{M}_I and the relation

$$\overline{M}_I = -1.74 + 0.14(\overline{N} - 20). \quad (4)$$

Again, there is some covariance between \overline{M}_I derived this way and \overline{m}_I , but this correlation has such a shallow slope that a distance modulus derived this way will suffer little in accuracy.

We do not want to suggest that use of \overline{N}

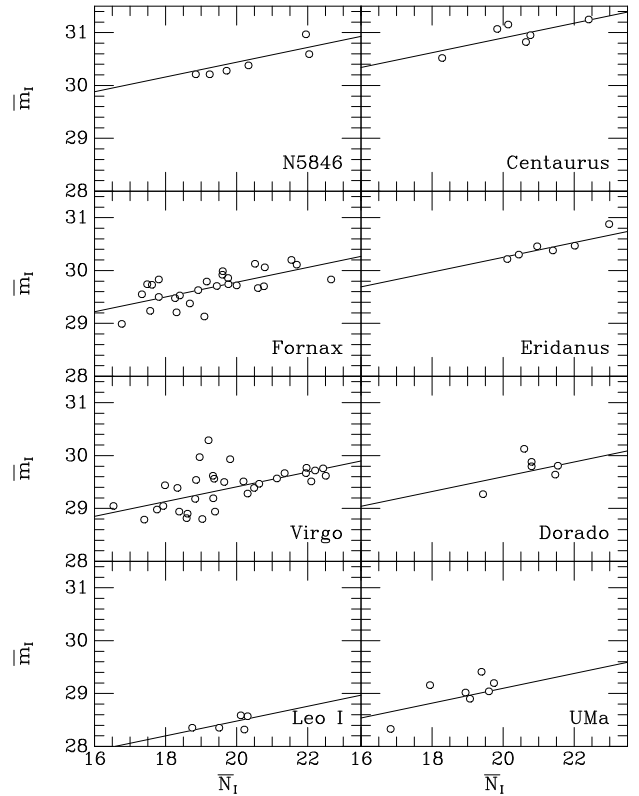


Fig. 5.— The fluctuation magnitude \overline{m}_I for SBF galaxies in eight selected groups is shown as a function of \overline{N}_I . The lines are *not* fitted to the data, but are drawn with a slope of 0.14 and zero points according to the SBF distance of the group derived from $(V-I)$ and \overline{m}_I .

should supplant the use of $(V-I)$ to derive \overline{M}_I . Use of $(V-I)$ has a solid basis on stellar populations whereas \overline{N} correlates with \overline{M}_I for similar reasons that elliptical galaxies fall on a fundamental plane, and potentially has unpleasant systematic problems. Although the relation between \overline{M}_I and \overline{N} shown in Figure 5 appears to track the relation between \overline{M}_I and $(V-I)$ in eight different groups, it would not be surprising if the \overline{M}_I - \overline{N} relation has environmental or type dependencies. We offer \overline{N} mainly as a simple and easy way to get a fairly reliable distance, and believe that it is a worthy subject for study in its own right. For example, Figure 6 illus-

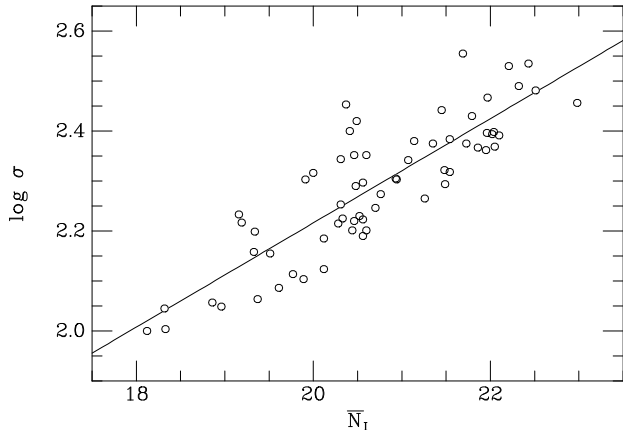


Fig. 6.— The velocity dispersion of elliptical SBF galaxies is shown as a function of \bar{N}_I .

trates the rather tight correlation between \bar{N} and central velocity dispersion, tabulated by Prugniel and Simien (1996):

$$\log \sigma = 2.22 + 0.10 (\bar{N} - 20). \quad (5)$$

7. Lessons Learned and Future SBF Possibilities

The SBF Survey was an unexpectedly large project. We condensed a total of 7828 CCD frames taken over 65 observing runs to 2646 independent images, comprising a total of 1022 hours of exposure time. Unfortunately, most of the integration time was spent on observations which eventually did not contribute to measurements of \bar{m}_I . Either the seeing was superseded by a later observation or the time was spent on photometry, as discussed below. The total observing time that resulted in the \bar{m}_I measurements of Table 1 amounted to only 370 hours.

Figure 7 shows the distribution of seeing during these observations.

Obviously, good seeing and high throughput are the keys to successful SBF measurements. If, for example, we were to take advantage of better seeing to redo the present survey, reaching $\text{PD} = 1.3$ by collecting $10 e^-$ per \bar{m}_I with a high-resistivity, near IR sensitive CCD and a wider-

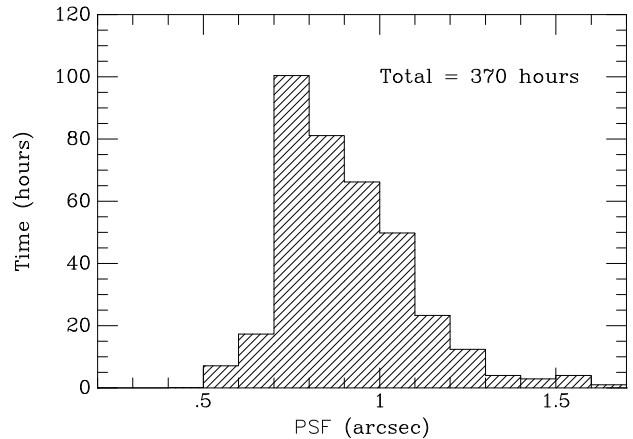


Fig. 7.— The number of hours of exposure time is shown as a function of seeing for the observations which eventually contributed to the tabulated values for \bar{m}_I .

bandpass, high throughput I filter (gaining us about a factor of two in sensitivity), we could redo the entire survey in about 100 hours on a 2.4-m telescope. Furthermore, this set of would distance measurements would be a factor of two better, with a median error in \bar{m}_I of ~ 0.12 mag.

Figure 8 shows the distribution of seeing we would require for this project.

Another major lesson learned concerned photometry. It is clear in hindsight that I-band SBF is very color sensitive, since the K and M giants that dominate the fluctuations are very red and have strong variations in (V-I) color. As a result, excellent photometry is mandatory for SBF. Our adopted program of “fitting in” photometric observations into our \bar{m}_I observations was not efficient. It would have been far better to devote all the good-seeing time on large telescopes for \bar{m}_I measurements and collect all the photometry on a few photometric, well-calibrated nights with a 1-m class telescope, with a common filter and CCD. As discussed in SBF-I, we encountered a particular problem calibrating I-band photometry with Tektronix CCDs which Sirianni et al. (1998) suggest is due to reflections from the mounting glass. This results in a large halo

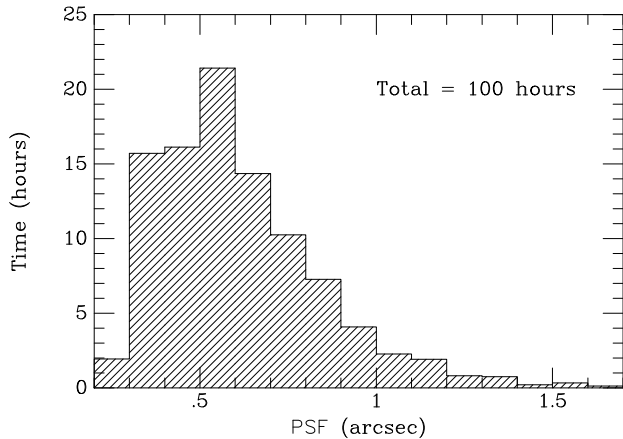


Fig. 8.— The number of hours of exposure time is shown as a function of seeing for a new set of observations which would improve the error in \overline{m}_I to a median of 0.12 mag.

around the psf which affects points sources (standard stars) more than extended sources (target galaxies).

Finally, better software could have helped. We certainly learned how best to carry out SBF reductions throughout the project, but software which was more automated would have meant that improvements could be easily applied to already reduced data. Some aspects of the software could stand improvement even today, particularly galaxy fitting. Improved analytic models of systems with embedded disks, for example, highly inclined S0 galaxies, would doubtless add more galaxies with good SBF determinations, since removal of such large-scale features is essential for a good measurement of the power spectrum on smaller scales. Our software is available on request to aid in the development of more refined SBF reduction packages.

These lessons would have greatly eased and improved our ground-based *I*-band SBF survey that we spent a decade completing, but we also believe that the true potential of the SBF technique lies ahead with new tools and applications. Our successful SBF observations have mostly been limited to galaxies with distances $D \lesssim 40$

Mpc. With the increased aperture size and better delivered image quality of the new generation of large telescopes it should be possible to push considerably further: in 0.4'' seeing it will be straightforward to get excellent measurements out beyond 50 Mpc. This is an interesting range for measuring large scale flows, near enough that an individual measurement has very good accuracy ($< 200 \text{ km s}^{-1}$), yet far enough to sample more than our local volume. (We also note that the accuracy of the distances we present here is limited mostly by observing conditions; we believe it would even be worthwhile to redo our survey given far superior observing conditions. Figure 8 is similar to the seeing distribution hoped for on the new generation of telescopes, and an aperture larger than 2.4-m would reduce the necessary exposure times proportionately.

Recent improvements in size and characteristics in IR arrays have opened the door for the SBF technique. It is possible that the near-IR will ultimately prove more powerful: the amplitude of the SBF signal is 20–40 times larger, the seeing is usually much better, and dust in the target galaxy is less of a problem. On the other hand, the much brighter sky detracts from these advantages, and there are concerns about variations in the stellar population, galaxy to galaxy, that may be more difficult to calibrate. Whereas the *I*-band is dominated by light from every main sequence star as it climbs the giant branch, in the *K*-band there is significant contribution from rarer AGB stars, which could make distance measurements sensitive to stochastic variations in intermediate-age populations. There is also substantial doubt as to whether near-IR SBF magnitudes for elliptical galaxies are more than a one-parameter family. According to Blakeslee et al. (2000), the stellar population models indicate that, at low metallicities, near-IR SBF magnitudes depend mainly on age, while integrated color depend mainly on metallicity. At higher metallicities, the SBF amplitudes plateau, leading to a more complicated relation between color

and \overline{M} . Depending upon the mixture of ages and metallicities occurring in actual galaxies, this relation might or might not be a simple one. Thus, an accurate characterization of near-IR SBF for a large and diverse sample of galaxies could be extremely important from the standpoint of both stellar population and distance studies.

The next generations of HST instruments (ACS, WFC3) should be superb for SBF surveys. The imaging quality of HST makes it possible to get good *I*-band SBF distances at $10,000 \text{ km s}^{-1}$. These new cameras will be much more sensitive in the red than WFPC2, so the exposure times will be shorter. The field of view will also be greater, giving more surface area for the measurement. Using the NICMOS camera SBF in the *H*-band can reach $10,000 \text{ km s}^{-1}$ in a single orbit, and a modern IR array in WFC3 would be even faster and better.

SBF has the potential to provide an accurate, unbiased chart of large-scale structure — defined by mass rather than galaxies — closer than $10,000 \text{ km s}^{-1}$. Apart from cosmological studies of H_0 , large scale flows, local inhomogeneities, biasing of galaxy density with respect to mass, this will provide an important data for understanding the physics of galaxy formation by relating galaxy properties to the large-scale distribution of dark matter. No longer limited by our inability to convert fluxes and angles to luminosities and distances, we will add needed precision into studies of the history of star formation and structure for the nearest galaxies, those that we can study best.

It is with great sadness that we acknowledge the tragic death of our good friend and colleague Jeffrey Willick during the preparation of this paper. Jeff's contributions to the study of large-scale flows have been an important influence on our work; he will be sorely missed.

We remain grateful to all our friends who have helped us collect these data over the years. Paul Schechter in particular has contributed many ob-

servations and much advice. Discussions with Nick Kaiser about variance of variance were extremely helpful. Thanks are due to Brian Barris for providing us with profile fits and magnitudes. This work was supported primarily by NSF grant AST9401519.

REFERENCES

- Ajhar, E. A., Lauer, T. R., Tonry, J. L., Blakeslee, J. P., Dressler, A., Holtzman, J. A., & Postman, M. 1997, *AJ*, 114, 626
- Bardeen, J.M., Bond, J.R., Kaiser, N., Szalay, A.S. 1986, *ApJ*, 304, 15.
- Bertelli, G., Bressan, A., Chiosi, C., Fagotto, F. & Nasi, E. 1994, *A&AS*, 106, 275
- Blakeslee, J. P., Ajhar, E. A., & Tonry, J. L. 1999, in *Post-Hipparcos Cosmic Candles*, eds. A. Heck & F. Caputo (Boston: Kluwer Academic Publishers), 181
- Blakeslee, J.P., Davis, M. Tonry, J.L., Dressler, A. & Ajhar, E.A. 1999, *ApJ*, 527, L73 (SBF-III)
- Blakeslee, J.P., Vazdekis, A. & Ajhar, E.A. 2000, *MNRAS*, in press (astro-ph/0008218)
- Bruzual, G. A. & Charlot, S. 1993, *ApJ*, 405, 538
- Burstein, D., & Heiles, C. 1984, *ApJS*, 54, 33 (BH)
- de Vaucouleurs, G., de Vaucouleurs, A., Corwin, H. G., Jr., Buta, R. J., Paturel, G., & Fouqué, P. 1991, *Third Reference Catalog of Bright Galaxies* (New York: Springer-Verlag) (RC3)
- Faber, S. M., Wegner, G., Burstein, D., Davies, R. L., Dressler, A., Lynden-Bell, D., & Terlevich, R. J. 1989, *ApJS*, 69, 763. (7S)
- Ferrarese, L., et al. 2000, *ApJ*, 529, 745
- Fisher, K.B., Huchra, J.P., Strauss, M.A., Davis, M., Yahil, A., & Schlegel, D. 1995, *ApJS*, 100, 69
- Freedman, W. L. et al. in preparation.
- Girardi, L., Bressan, A., Bertelli, G. & Chiosi, C. 2000, *A&AS*, 141, 371
- Herrnstein, J. R., et al. 1999, *Nature*, 400, 539
- Hudson, M. J., Smith, R. J., Lucey, J. R., Schlegel, D. G., & Davies, R. L. 1999, *ApJ*, 512, L79
- Jensen, J. B., Luppino, G. A., & Tonry, J. L. 1998a, *ApJ*, 505, 111
- Jensen, J. B., Luppino, G. A., & Tonry, J. L. 1998b, *ApJ*, 510, 71
- Kelson, D., et al. 2000, *ApJ*, 529, 768
- Laney, C. D. & Stobie, R. S. 1994, *MNRAS*, 266, 441
- Lauer, T. R., & Postman, M. 1994, *ApJ*, 425, 418
- Lauer, T. R., Tonry, J. L., Postman, M., Ajhar, E. A., & Holtzman, J. A. 1998, *ApJ*, 499, 577
- Layden, A. C., Hanson, R. B., Hawley, S. L., Klemola, A. R. & Hanley, C.J. 1996, *AJ*, 112, 2110
- Liu, M.C., Charlot, S. & Graham, J.R. 2000, *ApJ*, in press (astro-ph/0004367)
- Maoz, E., et al. 1999, *Nature*, 401, 351
- Mould, J. R., et al. 2000, *ApJ*, 529, 786
- Pahre, M. A., et al. 1999, *ApJ*, 515, 79
- Prugniel, P., & Simien, F., 1996 *A&AS*, 309, 749.
- Santiago, B.X., Strauss, M.A., Lahav, O., Davis, M., Dressler, A., & Huchra, J.P. 1995, *ApJ*, 446, 457
- Scaramella, R., Baiesi-Pillastrini, G., Chincarini, G., Vettolani, G., & Zamorani, G. 1989, *Nature*, 338, 562
- Schlegel, D. J., Finkbeiner, D. P., & Davis, M. 1998, *ApJ*, 500, 525 (SFD)
- Sirianni, M., Clampin, M., Hartig, G.F., Rafal, M.D., Ford, H.C., Golimowski, D.A., Tremonti, C., Illingworth, G., Blouke, M.M.,

Lesser, M.P., Burmester, W., Kimble, R.A., Sullivan, P.; Krebs, C.A., Yagelowicz, J., 1998, Proc. SPIE Vol. 3355, 608.

Tonry, J.L. 1991, ApJ, 373, L1.

Tonry, J.L., Ajhar, E.A., & Luppino, G.A. 1990, AJ, 100, 1416.

Tonry, J. L., Blakeslee, J. P., Ajhar, E. A., & Dressler, A. 1997, ApJ, 475, 399 (SBF-I)

Tonry, J. L., Blakeslee, J. P., Ajhar, E. A., & Dressler, A. 2000, ApJ, 530, 625 (SBF-II)

Willick, J. A. 1999, ApJ, 522, 647

Willick, J.A. & Batra, P. 2000, ApJ, submitted, astro-ph/0005112

Worthey, G. 1993a, ApJ, 409, 530

Worthey, G. 1993b, ApJ, 418, 947

Worthey, G. 1994, ApJS, 95, 107

TABLE 1
SBF DATA

Galaxy	RA	Dec	v_{CMB}	T	Grp	A_B	$(V-I)$	\bar{m}_I	$(m-M)$	$\langle r \rangle$	Q	PD	\bar{N}_I
N7814	0.813	16.146	684	2	0	0.19	1.245 0.017 2	29.29 0.10 2	30.60 0.14	36 0.4 2.4	8.3	0.51	20.3
N0063	4.440	11.449	803	0	0	0.48	0.979 0.018 2	28.85 0.31 1	31.36 0.33	24 0.6 1.3	5.4	1.14	17.8
N0147	8.298	48.508	-456	-5	282	0.75	1.024 0.009 3	22.13 0.15 2	24.44 0.16	35 0.0 5.0	9.9	0.01	13.6
N0185	9.742	48.338	-494	-5	282	0.79	1.051 0.017 4	21.83 0.13 3	24.02 0.16	43 0.0 4.1	9.9	0.01	14.2
N0221	10.675	40.865	-494	-6	282	0.35	1.133 0.007 6	22.73 0.05 3	24.55 0.08	30 0.0 5.9	9.9	0.01	15.6
N0224	10.685	41.269	-590	3	282	0.35	1.231 0.007 5	23.03 0.05 3	24.40 0.08	51 0.0 3.4	9.9	0.01	21.6
N0274	12.758	-7.058	1390	-3	0	0.24	1.135 0.020 2	29.64 0.45 1	31.45 0.47	33 0.7 1.4	3.0	1.68	18.8
N0404	17.363	35.718	-332	-3	0	0.25	1.054 0.011 2	25.40 0.07 2	27.57 0.10	23 0.0 3.8	9.9	0.01	16.9
N0448	18.816	-1.625	1589	-3	0	0.26	1.132 0.029 1	30.58 0.33 1	32.41 0.35	18 0.4 1.6	4.3	1.41	19.3
N0524	21.199	9.539	2091	-1	0	0.36	1.221 0.010 3	30.48 0.19 1	31.90 0.20	64 0.7 1.4	2.6	1.65	21.6
N0584	22.837	-6.868	1566	-5	26	0.18	1.157 0.009 4	29.82 0.19 2	31.52 0.20	23 0.3 3.4	3.1	1.41	20.6
N0596	23.217	-7.033	1509	-4	26	0.16	1.135 0.008 5	29.89 0.08 2	31.69 0.10	31 0.2 2.5	3.1	1.51	20.3
N0636	24.778	-7.513	1504	-5	26	0.11	1.156 0.008 5	30.65 0.14 1	32.37 0.16	19 0.4 3.0	3.8	1.13	20.6
N0720	28.252	-13.739	1438	-5	0	0.07	1.214 0.009 4	30.76 0.15 1	32.21 0.17	32 0.2 1.8	4.0	1.09	21.7
N0821	32.088	10.996	1433	-5	0	0.47	1.196 0.022 1	30.38 0.13 1	31.91 0.17	30 0.5 2.2	5.3	1.00	20.9
N0855	33.515	27.877	338	-5	0	0.31	1.015 0.018 1	27.59 0.14 2	29.94 0.17	19 0.5 1.8	9.6	0.23	16.2
N0891	35.638	42.347	305	3	0	0.28	1.142 0.017 1	27.83 0.11 1	29.61 0.14	94 0.5 1.9	9.6	0.36	19.3
N0936	36.907	-1.155	1176	-1	0	0.15	1.213 0.010 3	30.35 0.28 1	31.81 0.28	49 0.7 1.3	5.4	0.94	21.8
N0949	37.704	37.136	381	3	0	0.25	0.958 0.011 2	27.65 0.16 1	30.26 0.18	35 0.6 1.2	9.3	0.44	17.0
N1023	40.100	39.063	432	-3	0	0.26	1.193 0.017 2	28.74 0.13 3	30.29 0.16	45 0.1 3.9	9.5	0.25	20.9
N1052	40.270	-8.256	1242	-5	207	0.12	1.213 0.010 3	29.98 0.26 2	31.44 0.27	46 0.4 1.7	3.5	1.48	20.8
N1162	44.733	-12.399	2126	-5	29	0.21	1.173 0.032 1	31.44 0.27 1	33.08 0.31	18 0.4 3.3	1.8	1.91	20.6
N1172	45.400	-14.837	1472	-4	29	0.28	1.112 0.032 1	29.75 0.13 1	31.66 0.20	23 0.3 2.5	3.8	1.40	19.4
N1199	45.910	-15.614	2512	-5	29	0.23	1.188 0.012 3	31.03 0.32 1	32.60 0.32	28 0.3 2.1	0.9	2.03	20.9
N1201	46.035	-26.068	1548	-2	0	0.07	1.178 0.009 3	29.91 0.29 1	31.53 0.30	44 0.7 1.4	1.9	2.04	20.5
N1209	46.513	-15.612	2429	-5	29	0.16	1.198 0.010 3	31.24 0.22 1	32.77 0.23	20 0.4 2.9	1.7	1.72	21.1
N1297	49.809	-19.101	1383	-2	0	0.12	1.187 0.018 2	30.70 0.41 1	32.28 0.42	44 0.7 1.4	3.4	1.42	20.3
N1316	50.673	-37.208	1657	-2	31	0.09	1.132 0.016 2	29.83 0.15 2	31.66 0.17	110 0.3 2.2	1.9	1.79	22.7
I1919	51.508	-32.896	1058	-3	31	0.06	1.108 0.018 1	29.38 0.14 1	31.31 0.17	16 0.4 1.8	5.5	0.85	18.7
N1332	51.572	-21.336	1316	-3	32	0.14	1.222 0.010 4	30.38 0.16 1	31.80 0.18	37 0.4 1.6	4.1	1.01	21.4
N1336	51.630	-35.714	1344	-3	31	0.05	1.124 0.032 1	29.53 0.15 2	31.38 0.21	34 0.2 1.7	3.7	1.45	18.4
E358-006	51.824	-34.527	1234	-4	31	0.04	1.068 0.020 2	29.24 0.31 1	31.35 0.32	13 0.6 2.2	4.8	0.97	17.6
N1339	52.027	-32.286	1252	-4	31	0.06	1.134 0.012 3	29.79 0.35 1	31.61 0.35	20 0.4 1.5	4.2	0.95	19.2
N1344	52.080	-31.068	1086	-5	31	0.08	1.135 0.011 3	29.67 0.29 2	31.48 0.30	27 0.3 2.2	5.0	0.97	20.6
N1351	52.645	-34.853	1420	-3	31	0.06	1.148 0.016 2	29.86 0.13 1	31.61 0.16	26 0.3 2.2	3.8	1.12	19.8
N1366	53.472	-31.193	1186	-2	31	0.07	1.095 0.018 1	29.63 0.27 1	31.62 0.29	22 0.7 1.4	3.6	1.48	18.9
N1373	53.745	-35.171	1272	-4	31	0.06	1.085 0.013 2	29.74 0.46 1	31.78 0.47	11 0.7 1.4	2.7	2.05	17.5
N1375	53.819	-35.266	660	-2	31	0.06	1.070 0.019 1	29.48 0.09 3	31.58 0.13	23 0.3 2.5	8.2	0.51	18.3
N1374	53.820	-35.226	1284	-5	31	0.06	1.146 0.016 2	29.72 0.10 1	31.48 0.13	37 0.2 3.1	4.3	1.00	20.0
E358-025	53.889	-32.465	1346	-3	31	0.04	1.034 0.018 1	28.99 0.24 1	31.25 0.26	23 0.7 1.3	2.4	2.07	16.8
N1379	54.014	-35.441	1297	-5	31	0.05	1.143 0.019 1	29.74 0.11 1	31.51 0.15	41 0.2 2.8	4.2	1.00	19.8
N1380	54.112	-34.976	1732	-2	31	0.08	1.197 0.019 1	29.70 0.15 2	31.23 0.18	49 0.3 2.4	0.8	2.67	20.8
N1381	54.131	-35.294	1640	-2	31	0.06	1.189 0.018 1	29.71 0.19 1	31.28 0.21	24 0.6 1.2	3.1	1.16	19.4
N1386	54.193	-35.999	815	-1	31	0.05	1.101 0.018 1	29.13 0.23 1	31.09 0.25	46 0.6 1.3	5.3	1.26	19.1
N1380A	54.197	-34.739	1485	-2	31	0.06	1.138 0.018 1	29.21 0.28 1	31.00 0.29	23 0.6 1.3	2.1	2.15	18.3
N1387	54.238	-35.506	1192	-3	31	0.06	1.208 0.047 2	30.06 0.14 1	31.54 0.26	26 0.3 2.2	4.3	1.16	20.8
N1382	54.285	-35.195	1652	-3	31	0.07	1.106 0.013 2	29.83 0.30 2	31.77 0.31	18 0.4 2.1	1.2	2.58	17.8
N1389	54.299	-35.745	841	-3	31	0.05	1.145 0.019 1	29.92 0.16 1	31.68 0.18	26 0.6 2.4	6.1	0.91	19.6
N1399	54.621	-35.449	1314	-5	31	0.06	1.227 0.016 2	30.11 0.13 1	31.50 0.16	46 0.2 2.6	3.8	1.34	21.7
N1395	54.623	-23.028	1568	-5	32	0.10	1.215 0.010 4	30.47 0.14 2	31.91 0.16	40 0.2 2.9	2.9	1.49	22.0
N1411	54.688	-44.100	910	-3	0	0.04	1.107 0.018 1	29.54 0.23 1	31.48 0.25	30 0.5 2.0	4.9	1.21	19.4
N1404	54.715	-35.593	1817	-5	31	0.05	1.224 0.016 2	30.20 0.16 1	31.61 0.19	45 0.3 2.7	2.0	2.00	21.5
N1400	54.880	-18.689	409	-3	32	0.28	1.170 0.009 4	30.46 0.32 3	32.11 0.33	34 0.4 2.3	9.6	0.32	21.0
N1407	55.052	-18.581	1627	-5	32	0.30	1.222 0.010 4	30.88 0.25 1	32.30 0.26	31 0.2 1.9	2.9	1.42	23.0
N1419	55.178	-37.512	1456	-5	31	0.06	1.110 0.018 1	29.50 0.22 1	31.42 0.24	22 0.7 1.4	2.8	1.63	17.8
N1427	55.582	-35.393	1326	-4	31	0.05	1.152 0.018 1	30.13 0.22 1	31.86 0.24	42 0.4 1.4	3.5	1.45	20.5
N1426	55.705	-22.110	1313	-5	32	0.07	1.161 0.009 4	30.22 0.17 1	31.91 0.18	29 0.2 2.0	4.3	1.27	20.1

TABLE 1—*Continued*

Galaxy	RA	Dec	v_{CMB}	T	Grp	A_B	$(V-I)$	\overline{m}_I	$(m-M)$	$\langle r \rangle$	Q	PD	\overline{N}_I
N1439	56.210	-21.922	1543	-5	32	0.13	1.131 0.009 4	30.30 0.13 1	32.13 0.15	28 0.3 2.1	3.3	1.25	20.4
E358-059	56.264	-35.973	931	-3	31	0.04	1.081 0.016 2	29.55 0.18 1	31.60 0.20	13 0.6 2.3	6.4	1.02	17.3
I2006	58.618	-35.967	1252	-5	31	0.05	1.183 0.018 1	29.99 0.27 1	31.59 0.29	45 0.7 1.4	3.6	1.45	19.6
N1527	62.102	-47.897	1117	-3	0	0.05	1.230 0.016 2	29.90 0.20 1	31.28 0.22	25 0.3 2.3	4.4	0.95	20.5
N1533	62.464	-56.121	744	-3	211	0.07	1.198 0.018 1	30.13 0.37 1	31.65 0.38	44 0.7 1.4	5.7	1.14	20.6
N1543	63.180	-57.737	1065	-2	211	0.12	1.173 0.016 2	29.88 0.14 1	31.51 0.17	52 0.3 2.2	4.2	1.11	20.8
N1537	63.421	-31.646	1300	-3	210	0.11	1.096 0.018 1	29.84 0.16 1	31.83 0.19	40 0.4 3.0	3.0	1.72	20.5
N1549	63.938	-55.592	1128	-5	211	0.05	1.168 0.016 2	29.81 0.15 1	31.47 0.18	24 0.3 2.4	3.5	1.13	21.5
N1553	64.043	-55.781	1256	-2	211	0.05	1.159 0.016 2	29.64 0.14 1	31.34 0.17	29 0.2 2.0	3.3	1.31	21.5
N1574	65.496	-56.974	1025	-3	211	0.07	1.162 0.016 2	29.80 0.19 1	31.49 0.21	35 0.4 1.7	4.0	1.10	20.8
N1596	66.907	-55.027	1508	-2	211	0.04	1.171 0.016 2	29.27 0.13 1	30.92 0.16	21 0.3 2.8	2.2	1.57	19.4
N2271	100.718	-23.476	2724	-3	0	0.53	1.234 0.029 1	31.15 0.25 1	32.51 0.28	21 0.4 2.8	1.9	1.93	20.6
N2293	101.929	-26.753	2135	-1	0	0.52	1.237 0.013 2	29.81 0.40 1	31.16 0.41	11 0.7 1.4	2.6	2.03	20.8
N2325	105.669	-28.697	2408	-5	0	0.51	1.164 0.014 2	30.36 0.14 1	32.04 0.16	19 0.3 2.3	2.1	2.14	21.3
N2380	110.980	-27.529	1963	-2	0	1.32	1.110 0.009 4	30.14 0.35 1	32.05 0.35	15 0.5 1.9	2.1	1.63	21.2
E208-021	113.486	-50.442	1166	-3	0	0.75	1.146 0.018 1	28.90 0.18 1	30.66 0.20	41 0.7 1.5	4.0	1.43	19.5
N2434	113.715	-69.284	1440	-5	212	1.07	1.098 0.055 1	29.70 0.15 1	31.67 0.29	27 0.3 2.2	4.1	1.43	20.6
I2311	124.690	-25.371	2090	-5	0	0.62	1.136 0.027 1	30.04 0.14 1	31.84 0.20	19 0.4 3.0	2.3	2.09	20.0
N2549	124.743	57.803	1159	-2	0	0.28	1.163 0.012 2	28.82 0.27 1	30.51 0.28	33 0.7 1.3	3.0	1.39	18.9
N2592	126.783	25.971	2213	-5	0	0.26	1.205 0.010 3	30.55 0.42 2	32.05 0.43	28 0.4 1.6	1.1	2.26	19.8
N2634	132.105	73.967	2309	-5	283	0.09	1.154 0.022 1	30.90 0.67 1	32.62 0.68	24 0.7 1.4	1.5	2.22	20.9
N2683	133.171	33.417	640	3	0	0.14	1.147 0.015 1	27.68 0.35 1	29.44 0.36	48 0.7 1.5	5.4	0.49	19.1
N2681	133.388	51.315	868	0	0	0.10	1.041 0.010 3	28.95 0.34 1	31.18 0.34	60 0.6 2.4	6.1	0.74	20.3
N2695	133.613	-3.067	2126	-2	273	0.08	1.183 0.051 1	30.96 0.32 2	32.55 0.40	20 0.3 2.9	3.1	1.64	20.3
N2699	133.953	-3.128	2128	-5	273	0.09	1.152 0.051 1	30.42 0.14 1	32.15 0.27	18 0.4 1.6	2.2	1.68	19.3
N2768	137.907	60.039	1483	-5	215	0.19	1.144 0.027 1	29.98 0.20 1	31.75 0.24	24 0.7 1.4	3.4	0.96	21.0
N2784	138.078	-24.173	1014	-2	0	0.93	1.188 0.023 1	28.40 0.23 2	29.96 0.25	54 0.3 2.2	4.4	1.37	20.3
N2778	138.102	35.028	2250	-5	216	0.09	1.150 0.015 1	30.06 0.29 1	31.80 0.30	18 0.5 2.0	1.5	2.07	18.7
N2787	139.829	69.203	763	-1	0	0.57	1.194 0.019 1	27.82 0.35 1	29.37 0.36	35 0.6 1.3	3.3	1.18	18.9
N2865	140.878	-23.163	2897	-5	284	0.36	1.105 0.019 2	30.95 0.17 1	32.89 0.20	21 0.3 2.8	0.6	2.14	20.8
N2880	142.396	62.490	1677	-3	215	0.14	1.148 0.015 1	29.95 0.20 1	31.70 0.21	22 0.4 1.6	2.9	1.31	19.4
N2904	142.570	-30.384	2694	-3	0	0.54	1.201 0.041 1	30.36 0.14 2	31.86 0.24	19 0.3 2.2	1.7	2.07	19.3
N2974	145.639	-3.700	2266	-5	0	0.23	1.203 0.015 1	30.16 0.23 1	31.66 0.24	37 0.6 2.4	0.6	2.15	21.0
N2950	145.652	58.852	1466	-2	0	0.07	1.110 0.019 1	28.95 0.25 1	30.87 0.27	33 0.7 1.3	1.0	2.23	19.3
N3032	148.033	29.237	1842	-2	0	0.07	1.073 0.019 1	29.62 0.26 1	31.71 0.28	25 0.7 1.4	2.7	1.71	18.8
N3056	148.637	-28.297	1373	-1	0	0.39	1.073 0.023 1	28.34 0.22 1	30.43 0.25	27 0.6 2.2	2.5	1.98	17.9
N3031	148.890	69.067	46	2	0	0.35	1.187 0.011 3	26.38 0.25 3	27.96 0.26	72 0.0 2.4	9.9	0.04	20.8
N3078	149.602	-26.926	2837	-5	219	0.31	1.209 0.017 2	31.25 0.29 2	32.73 0.30	31 0.5 2.0	1.0	2.67	21.6
N3087	149.787	-34.225	2976	-4	218	0.45	1.164 0.019 2	31.04 0.18 1	32.72 0.21	23 0.3 2.6	1.6	2.23	21.2
N3073	150.216	55.620	1317	-3	0	0.04	1.007 0.019 1	30.26 0.92 1	32.64 0.93	17 0.7 1.3	1.9	1.51	18.3
N3077	150.838	68.734	95	0	0	0.29	1.044 0.015 2	25.81 0.10 1	28.03 0.13	46 0.4 2.9	9.9	0.09	17.1
N3115	151.309	-7.719	1054	-3	0	0.20	1.183 0.010 6	28.34 0.06 4	29.93 0.09	54 0.3 3.2	4.4	0.95	20.8
N3136	151.451	-67.378	1823	-5	44	1.03	1.095 0.033 2	29.96 0.15 1	31.95 0.22	32 0.5 1.9	3.5	1.39	21.2
N3136B	152.555	-67.005	1949	-4	44	0.81	1.164 0.033 2	29.96 0.11 2	31.64 0.19	17 0.4 3.4	3.1	1.52	19.6
N3156	153.171	3.131	1651	-2	252	0.15	1.011 0.011 5	29.38 0.13 1	31.75 0.14	17 0.4 1.7	3.0	1.34	18.5
N3193	154.604	21.895	1696	-5	45	0.11	1.174 0.009 4	31.03 0.17 1	32.66 0.18	23 0.2 3.0	3.8	0.85	21.5
N3226	155.864	19.899	1601	-5	45	0.10	1.178 0.015 1	30.25 0.23 1	31.86 0.24	23 0.5 1.9	2.7	1.33	20.5
N3250	156.635	-39.943	3189	-5	46	0.44	1.226 0.019 3	31.75 0.14 2	33.15 0.17	27 0.3 2.2	1.6	2.14	22.1
N3245	156.826	28.508	1657	-2	0	0.11	1.139 0.023 1	29.81 0.16 1	31.60 0.20	25 0.4 1.7	1.2	1.79	20.0
N3257	157.196	-35.658	3344	-3	46	0.33	1.192 0.041 1	31.13 0.18 1	32.68 0.26	15 0.5 2.0	1.2	2.61	19.8
N3258	157.226	-35.606	3129	-5	46	0.36	1.209 0.034 1	31.06 0.22 1	32.53 0.27	26 0.3 2.3	1.7	2.32	21.2
N3268	157.503	-35.325	3084	-5	46	0.45	1.189 0.023 2	31.14 0.22 1	32.71 0.25	9 0.5 1.9	1.7	1.85	21.6
N3318	159.315	-41.628	3071	3	0	0.34	1.073 0.101 1	30.61 0.19 1	32.70 0.49	18 0.3 2.3	1.1	2.06	20.1
N3368	161.688	11.821	1252	2	57	0.11	1.145 0.015 1	28.32 0.20 1	30.08 0.22	132 0.7 1.3	1.7	1.63	20.2
N3377	161.924	13.983	1038	-5	57	0.15	1.114 0.009 4	28.35 0.06 3	30.25 0.09	42 0.2 3.7	4.8	0.89	19.5
N3379	161.958	12.582	1274	-5	57	0.10	1.193 0.015 1	28.57 0.07 2	30.12 0.11	57 0.2 3.1	2.4	1.59	20.3
N3384	162.072	12.630	1080	-3	57	0.11	1.151 0.018 1	28.59 0.10 1	30.32 0.14	63 0.3 2.4	3.9	1.24	20.1

TABLE 1—*Continued*

Galaxy	RA	Dec	v_{CMB}	T	Grp	A_B	$(V-I)$	\bar{m}_I	$(m-M)$	$\langle r \rangle$	Q	PD	\bar{N}_I
N3412	162.722	13.413	1218	-2	57	0.12	1.111 0.015 1	28.35 0.11 1	30.27 0.14	40 0.6 2.2	3.0	1.40	18.7
N3414	162.818	27.976	1784	-2	0	0.10	1.149 0.019 1	30.27 0.32 1	32.01 0.33	32 0.7 1.4	1.2	1.66	20.6
N3457	163.703	17.622	1497	0	0	0.14	1.098 0.015 1	29.60 0.13 2	31.58 0.15	17 0.5 2.1	3.4	1.32	18.2
N3489	165.076	13.902	1045	-1	0	0.07	1.041 0.023 1	28.18 0.10 2	30.41 0.15	49 0.4 1.4	3.9	0.96	18.9
N3557	167.490	-37.538	3337	-5	154	0.43	1.183 0.016 1	31.72 0.20 1	33.30 0.22	20 0.3 2.1	1.7	2.67	23.0
N3585	168.320	-26.756	1845	-5	285	0.28	1.160 0.016 2	29.81 0.16 1	31.51 0.18	56 0.5 2.1	1.2	2.31	21.5
N3599	168.864	18.113	1192	-2	48	0.09	1.112 0.012 2	29.63 0.16 1	31.54 0.18	27 0.4 1.6	4.4	1.14	19.3
N3605	169.195	18.018	1029	-5	48	0.09	1.118 0.024 2	29.70 0.27 1	31.58 0.29	8 0.7 1.4	5.1	1.11	18.1
N3607	169.225	18.053	1294	-2	48	0.09	1.152 0.010 3	30.06 0.15 1	31.79 0.17	32 0.3 2.7	3.8	1.40	21.4
N3608	169.245	18.149	1539	-5	48	0.09	1.156 0.009 5	30.09 0.12 1	31.80 0.14	25 0.2 2.7	3.8	0.92	20.5
N3610	169.608	58.787	1922	-5	281	0.04	1.108 0.015 1	29.73 0.20 1	31.65 0.22	32 0.7 1.4	0.7	2.21	19.8
N3613	169.651	58.001	2216	-5	281	0.05	1.175 0.015 1	30.69 0.39 1	32.32 0.40	27 0.4 1.6	0.3	2.22	21.0
N3626	170.015	18.358	1815	-1	48	0.09	1.009 0.015 1	29.13 0.23 1	31.51 0.24	52 0.7 1.4	1.6	2.03	19.2
N3640	170.278	3.236	1674	-5	50	0.19	1.140 0.009 5	30.37 0.12 1	32.16 0.13	25 0.3 2.3	3.1	1.49	21.3
N3641	170.286	3.195	2130	-5	50	0.18	1.131 0.012 3	30.30 0.24 1	32.13 0.25	16 0.4 1.8	1.8	1.90	18.7
N3818	175.489	-6.156	1874	-5	153	0.16	1.124 0.015 1	30.94 0.60 1	32.80 0.61	32 0.7 1.4	2.5	1.69	20.3
N3904	177.305	-29.276	2095	-5	52	0.31	1.156 0.055 1	30.55 0.13 1	32.26 0.28	26 0.3 2.2	2.7	1.51	21.0
N3923	177.759	-28.806	1953	-5	52	0.36	1.194 0.055 1	30.26 0.12 1	31.80 0.28	42 0.2 2.8	2.7	1.50	21.9
N3928	177.946	48.681	1187	3	155	0.09	1.096 0.015 1	29.16 0.63 1	31.14 0.64	20 0.6 2.2	2.5	1.47	17.9
N3941	178.230	36.987	1215	-2	0	0.09	1.125 0.013 2	28.58 0.16 1	30.43 0.18	48 0.1 1.9	1.3	1.63	19.3
I0745	178.551	0.136	1506	-2	0	0.09	0.978 0.010 4	28.80 0.30 1	31.31 0.30	17 0.6 1.3	0.2	2.33	16.8
N3990	179.401	55.459	879	-3	155	0.07	1.151 0.019 1	28.33 0.27 1	30.06 0.28	11 0.5 2.0	4.2	0.98	16.8
N3998	179.486	55.454	1202	-2	155	0.07	1.194 0.011 3	29.20 0.18 1	30.75 0.19	34 0.3 2.6	2.4	1.35	19.7
N4026	179.857	50.962	1077	-2	155	0.09	1.174 0.015 1	29.04 0.26 1	30.67 0.28	26 0.7 1.3	4.7	0.86	19.6
N4033	180.145	-17.842	1886	-5	53	0.20	1.113 0.023 1	29.71 0.20 1	31.62 0.23	22 0.7 1.4	1.2	2.56	19.3
N4105	181.670	-29.762	2222	-5	49	0.26	1.171 0.017 2	30.47 0.14 1	32.12 0.17	34 0.2 1.8	2.4	1.89	21.5
N4111	181.761	43.067	1045	-1	155	0.06	1.096 0.015 1	28.90 0.22 1	30.88 0.23	34 0.6 1.3	3.9	1.20	19.1
N4125	182.030	65.173	1455	-5	54	0.08	1.174 0.011 2	30.26 0.24 1	31.89 0.25	52 0.2 1.7	2.3	1.86	21.9
N4138	182.378	43.688	1070	-1	155	0.06	1.164 0.013 2	29.02 0.25 1	30.70 0.26	37 0.6 1.2	3.0	1.01	18.9
N4143	182.402	42.536	1207	-2	155	0.05	1.181 0.015 1	29.41 0.17 1	31.01 0.19	24 0.4 1.8	3.0	1.38	19.4
N4150	182.640	30.402	538	-2	55	0.08	1.071 0.017 1	28.60 0.22 1	30.69 0.24	33 0.7 1.3	6.3	0.81	18.3
N4203	183.772	33.198	1399	-3	0	0.05	1.195 0.019 1	29.36 0.15 1	30.90 0.18	39 0.3 2.2	1.9	1.26	20.7
N4251	184.533	28.176	1367	-2	55	0.10	1.117 0.015 1	29.57 0.18 1	31.46 0.20	35 0.3 2.5	2.9	1.41	20.0
N4258	184.741	47.304	664	4	0	0.07	1.134 0.023 1	27.50 0.08 2	29.31 0.14	103 0.7 1.7	6.3	0.61	21.1
N4261	184.845	5.827	2557	-5	150	0.08	1.258 0.014 2	31.25 0.18 1	32.50 0.19	25 0.2 2.7	1.0	1.28	22.3
N4278	185.030	29.280	938	-5	55	0.12	1.161 0.012 4	29.34 0.18 1	31.03 0.20	40 0.4 1.8	5.9	0.66	20.4
N4291	185.076	75.373	1765	-5	98	0.16	1.175 0.017 1	30.47 0.31 1	32.09 0.32	33 0.3 2.1	2.2	1.68	20.4
N4283	185.087	29.311	1371	-5	55	0.11	1.178 0.010 3	29.37 0.18 1	30.98 0.19	18 0.6 2.2	2.4	1.65	18.3
N4346	185.867	46.994	977	-2	0	0.06	1.158 0.012 2	29.07 0.15 1	30.78 0.17	31 0.7 1.4	4.0	1.00	19.1
N4339	185.893	6.082	1653	-5	56	0.11	1.200 0.015 1	29.56 0.16 1	31.08 0.18	21 0.5 2.1	1.1	2.07	19.4
N4365	186.116	7.318	1592	-5	150	0.09	1.222 0.017 1	30.14 0.14 1	31.55 0.17	35 0.3 2.5	3.0	1.35	21.8
N4386	186.122	75.530	1698	-2	0	0.17	1.196 0.019 1	30.63 0.48 1	32.16 0.49	34 0.6 1.3	2.4	1.87	20.3
N4374	186.265	12.887	1375	-5	56	0.17	1.191 0.008 5	29.77 0.09 2	31.32 0.11	55 0.2 2.8	4.1	1.30	22.0
N4379	186.312	15.608	1407	-3	56	0.10	1.185 0.017 1	29.18 0.39 1	30.76 0.41	28 0.4 1.6	2.4	1.42	18.8
N4391	186.329	64.934	1451	-3	54	0.08	1.112 0.015 1	29.99 0.26 1	31.90 0.27	16 0.7 1.4	3.2	1.38	18.5
N4382	186.353	18.191	1087	-1	0	0.13	1.150 0.022 3	29.59 0.09 2	31.33 0.14	53 0.1 2.7	5.5	0.76	21.8
E322-008	186.407	-39.320	3335	-2	35	0.36	1.205 0.023 2	31.37 0.50 1	32.86 0.52	21 0.7 1.4	0.0	2.53	20.7
N4387	186.424	12.812	925	-5	56	0.14	1.163 0.011 2	29.97 0.72 1	31.65 0.73	15 0.4 1.4	3.0	1.46	19.0
N4406	186.549	12.947	120	-5	56	0.13	1.167 0.008 5	29.51 0.12 1	31.17 0.14	27 0.2 2.8	5.7	0.85	22.1
N4419	186.737	15.048	154	1	56	0.14	1.126 0.026 2	28.80 0.21 1	30.65 0.25	49 0.4 1.4	2.5	1.15	19.0
N4441	186.837	64.800	1553	-1	0	0.09	1.005 0.012 2	29.00 0.44 1	31.40 0.45	32 0.7 1.4	1.5	1.51	17.2
N4434	186.904	8.155	1418	-5	56	0.10	1.125 0.015 1	30.29 0.15 1	32.14 0.17	12 0.6 2.2	6.9	0.61	19.2
I3370	186.904	-39.338	3276	-5	35	0.40	1.185 0.022 3	30.56 0.14 1	32.14 0.17	19 0.3 2.2	0.9	2.69	20.9
N4460	187.192	44.863	782	-1	0	0.08	1.011 0.015 1	27.54 0.17 1	29.91 0.19	33 0.7 1.4	5.6	0.88	16.8
N4458	187.241	13.243	1001	-5	56	0.10	1.140 0.011 2	29.39 0.09 1	31.18 0.12	15 0.4 1.8	6.8	0.66	18.3
N4459	187.250	13.979	1553	-1	56	0.20	1.187 0.015 1	29.47 0.21 1	31.04 0.22	37 0.2 1.9	3.5	1.11	20.6
N4468	187.380	14.050	1232	-3	56	0.20	1.045 0.015 1	28.79 0.11 1	31.00 0.14	19 0.5 2.0	3.1	1.35	17.4

TABLE 1—*Continued*

Galaxy	RA	Dec	v_{CMB}	T	Grp	A_B	$(V-I)$	\bar{m}_I	$(m-M)$	$\langle r \rangle$	Q	PD	\bar{N}_I
N4472	187.444	7.999	1346	-5	56	0.10	1.218 0.011 3	29.62 0.07 2	31.06 0.10	65 0.2 2.7	3.8	1.08	22.5
N4473	187.453	13.430	2575	-5	56	0.12	1.158 0.012 2	29.28 0.11 1	30.98 0.13	35 0.3 2.2	2.5	1.62	20.3
N4476	187.495	12.348	2296	-3	56	0.12	1.048 0.017 1	28.98 0.14 1	31.18 0.17	20 0.6 2.2	2.1	1.40	17.8
N4478	187.572	12.329	1711	-5	56	0.11	1.164 0.019 3	29.62 0.26 1	31.29 0.28	19 0.6 2.4	3.0	1.49	19.3
N4486	187.707	12.390	1632	-4	56	0.10	1.244 0.012 3	29.72 0.14 2	31.03 0.16	53 0.1 3.3	4.4	0.74	22.2
N4489	187.718	16.759	1290	-5	56	0.12	1.046 0.015 1	29.05 0.13 1	31.26 0.15	15 0.6 1.3	3.3	1.48	17.9
N4494	187.851	25.774	1653	-5	235	0.09	1.139 0.010 3	29.38 0.08 1	31.16 0.11	27 0.2 2.5	3.2	0.91	20.6
N4526	188.512	7.700	949	-2	56	0.10	1.188 0.021 4	29.57 0.17 2	31.14 0.20	46 0.2 3.8	5.3	0.92	21.1
N4531	188.567	13.076	345	-1	56	0.18	1.100 0.015 1	28.94 0.20 1	30.91 0.22	42 0.4 1.7	3.2	1.19	19.4
N4548	188.860	14.497	884	3	56	0.16	1.148 0.019 1	29.67 0.53 1	31.42 0.54	24 0.4 1.5	3.1	1.19	22.0
N4546	188.873	-3.794	1395	-3	0	0.15	1.155 0.013 2	29.03 0.19 1	30.74 0.20	34 0.3 2.1	2.9	1.20	19.7
N4550	188.879	12.221	719	-2	56	0.17	1.078 0.011 2	28.94 0.18 1	31.00 0.20	22 0.4 1.6	3.5	1.11	18.4
U07767	188.886	73.675	1390	-5	0	0.09	1.152 0.019 1	30.48 0.96 1	32.22 0.97	18 0.6 1.3	2.2	1.67	18.3
N4551	188.909	12.266	1536	-5	56	0.17	1.170 0.009 3	29.54 0.16 2	31.19 0.17	22 0.4 1.7	3.8	1.05	18.9
N4552	188.916	12.557	660	-5	56	0.18	1.194 0.015 1	29.39 0.11 1	30.93 0.14	59 0.3 2.6	3.1	1.35	20.5
N4565	189.086	25.989	1527	3	235	0.07	1.128 0.027 1	29.37 0.11 1	31.21 0.17	54 0.6 1.2	3.2	0.99	21.1
N4564	189.113	11.439	1504	-5	56	0.15	1.161 0.009 3	29.19 0.16 2	30.88 0.17	26 0.3 2.7	3.2	1.12	19.3
N4589	189.357	74.195	2040	-5	98	0.12	1.180 0.015 1	30.10 0.20 1	31.71 0.22	28 0.3 2.5	1.2	1.98	20.5
N4578	189.378	9.555	2626	-2	56	0.09	1.127 0.015 1	29.50 0.10 1	31.34 0.13	26 0.4 3.0	3.6	1.12	19.7
E322-038	189.576	-41.501	3428	-3	58	0.56	1.242 0.051 1	31.15 0.25 1	32.48 0.34	11 0.7 1.4	0.2	2.37	20.1
N4594	189.997	-11.623	1483	1	0	0.22	1.175 0.031 2	28.32 0.10 1	29.95 0.18	48 0.7 1.4	2.6	1.04	21.6
N4600	190.094	3.120	1137	-2	0	0.12	1.141 0.017 1	27.55 0.20 1	29.33 0.22	30 0.7 1.5	1.7	1.66	16.0
I3653	190.316	11.387	940	0	56	0.14	1.139 0.017 1	29.05 0.44 1	30.84 0.45	11 0.5 2.0	2.8	1.28	16.5
N4620	190.499	12.943	1511	-2	56	0.13	1.048 0.019 1	29.44 0.29 1	31.64 0.30	16 0.7 1.4	2.3	1.51	18.0
N4621	190.510	11.647	780	-5	56	0.14	1.172 0.018 2	29.67 0.18 1	31.31 0.20	48 0.2 3.2	2.5	1.62	21.4
N4616	190.571	-40.642	4880	-4	59	0.55	1.196 0.021 2	31.45 0.21 1	32.98 0.24	17 0.4 1.8	1.4	2.36	20.3
N4638	190.699	11.443	1484	-3	56	0.11	1.149 0.013 2	29.93 0.25 1	31.68 0.26	26 0.7 1.4	3.0	1.23	19.8
N4636	190.707	2.688	1286	-5	152	0.12	1.233 0.012 2	29.46 0.11 1	30.83 0.13	43 0.2 3.6	3.3	1.29	21.7
N4649	190.918	11.549	1430	-5	56	0.12	1.232 0.023 2	29.76 0.09 1	31.13 0.15	35 0.2 1.9	3.8	0.86	22.4
N4645	191.041	-41.750	2883	-4	58	0.64	1.188 0.025 2	30.82 0.13 1	32.38 0.18	17 0.3 2.5	1.9	2.13	20.6
N4660	191.135	11.191	1451	-5	56	0.14	1.154 0.015 1	28.82 0.17 1	30.54 0.19	26 0.4 1.7	2.3	1.67	18.6
N4684	191.824	-2.727	1940	-1	151	0.12	1.100 0.015 1	28.68 0.17 1	30.65 0.19	30 0.4 1.5	0.4	2.68	18.4
E322-088	192.091	-41.714	2895	-2	58	0.48	1.156 0.034 1	31.07 0.65 1	32.78 0.67	34 0.4 1.8	1.2	2.46	19.8
N4697	192.150	-5.801	1561	-5	151	0.13	1.157 0.010 3	28.64 0.12 1	30.35 0.14	41 0.3 2.1	1.7	2.19	20.8
N4696	192.208	-41.311	3248	-4	58	0.49	1.203 0.014 3	31.25 0.15 2	32.75 0.17	57 0.3 2.1	0.7	2.53	22.4
E322-101	192.391	-41.056	2343	0	58	0.49	1.167 0.023 2	30.52 0.42 1	32.18 0.44	10 0.5 2.1	2.7	1.99	18.3
N4709	192.517	-41.382	4939	-5	59	0.51	1.199 0.011 4	31.22 0.22 1	32.74 0.23	26 0.2 3.0	2.4	1.80	21.9
N4725	192.612	25.500	1502	2	0	0.05	1.209 0.023 1	29.14 0.32 1	30.61 0.34	27 0.7 1.3	2.1	1.82	21.8
N4736	192.723	41.119	540	2	0	0.08	1.071 0.017 1	26.49 0.15 2	28.58 0.18	123 0.6 1.4	6.2	0.52	19.3
N4733	192.779	10.912	1237	-4	56	0.09	1.099 0.015 1	28.90 0.18 1	30.87 0.20	26 0.3 2.7	3.9	1.03	18.6
N4742	192.950	-10.455	1669	-5	0	0.18	1.045 0.017 2	28.74 0.13 1	30.95 0.16	33 0.5 1.8	2.1	1.84	18.5
N4754	193.074	11.314	1705	-3	56	0.14	1.178 0.011 2	29.51 0.12 1	31.13 0.14	33 0.3 2.6	1.7	1.82	20.2
N4753	193.095	-1.199	1635	0	0	0.15	1.087 0.013 2	29.83 0.17 1	31.86 0.19	67 0.7 1.3	1.1	1.67	21.4
E323-034	193.358	-41.204	4542	-5	59	0.54	1.165 0.019 2	31.02 0.20 1	32.69 0.22	27 0.5 2.2	1.1	2.51	20.8
N4802	193.957	-12.055	1358	-2	0	0.21	1.004 0.018 1	27.92 0.13 1	30.31 0.16	28 0.7 1.4	2.2	1.63	17.7
N4826	194.185	21.685	717	2	0	0.18	1.029 0.011 2	27.09 0.18 1	29.37 0.20	102 0.7 1.4	5.4	0.77	19.9
N4946	196.372	-43.591	3310	-4	62	0.47	1.190 0.021 2	31.83 0.14 2	33.39 0.17	15 0.3 2.8	1.9	2.45	21.3
N5044	198.850	-16.386	3033	-5	63	0.30	1.210 0.027 1	31.00 0.25 1	32.47 0.28	28 0.3 2.4	0.3	2.18	21.2
N5102	200.491	-36.630	706	-3	226	0.24	0.976 0.016 1	25.49 0.09 1	28.01 0.13	57 0.3 2.1	5.3	0.90	17.6
N5128	201.371	-43.017	812	-2	226	0.50	1.078 0.016 1	26.05 0.11 1	28.12 0.14	185 0.6 1.3	4.4	1.07	21.8
N5195	202.495	47.272	742	0	0	0.16	1.056 0.019 1	27.25 0.25 2	29.42 0.27	38 0.0 1.9	6.0	0.63	19.4
N5273	205.535	35.653	1313	-2	0	0.04	1.142 0.017 1	29.31 0.24 1	31.09 0.26	26 0.4 1.7	2.2	1.38	18.9
N5322	207.315	60.191	1916	-5	254	0.06	1.183 0.011 2	30.88 0.22 1	32.47 0.23	29 0.4 3.0	1.0	1.74	22.0
N5338	208.360	5.208	1068	-2	0	0.12	1.019 0.023 1	28.21 0.28 1	30.54 0.30	14 0.5 1.1	3.0	2.05	16.8
N5485	211.798	55.002	2111	-2	237	0.07	1.180 0.017 1	30.46 0.33 1	32.07 0.34	32 0.7 1.4	0.6	2.32	20.5
N5582	215.181	39.693	1492	-5	0	0.06	1.145 0.013 2	30.51 0.22 1	32.27 0.23	24 0.5 1.8	3.8	1.21	20.1
N5574	215.235	3.239	1845	-3	0	0.14	1.054 0.011 3	29.71 0.61 1	31.89 0.62	17 0.6 1.3	1.2	2.18	18.4

TABLE 1—*Continued*

Galaxy	RA	Dec	v_{CMB}	T	Grp	A_B	($V-I$)	\bar{m}_I	($m-M$)	$\langle r \rangle$	Q	PD	\bar{N}_I
N5576	215.268	3.271	1818	-5	68	0.14	1.098 0.010 4	30.05 0.12 1	32.03 0.14	24 0.3 2.4	2.7	1.71	20.8
N5611	216.022	33.049	2154	-2	0	0.05	1.111 0.017 2	30.09 0.45 1	32.01 0.46	15 0.7 1.4	0.8	2.37	18.4
N5631	216.639	56.583	2057	-2	0	0.09	1.122 0.019 1	30.35 0.22 1	32.22 0.24	32 0.7 1.4	1.1	2.41	20.3
N5638	217.419	3.234	1901	-5	68	0.14	1.169 0.011 3	30.44 0.23 2	32.10 0.24	25 0.2 3.5	2.0	1.79	20.5
N5687	218.722	54.476	2310	-3	0	0.05	1.174 0.013 2	30.60 0.50 1	32.23 0.51	16 0.7 1.4	0.2	2.68	20.2
N5770	223.313	3.960	1687	-2	0	0.17	1.120 0.017 1	29.52 0.28 1	31.39 0.29	32 0.7 1.4	1.7	1.97	18.8
N5812	225.232	-7.458	2286	-5	0	0.38	1.213 0.015 1	30.70 0.28 1	32.15 0.29	33 0.3 2.6	0.8	2.35	21.2
N5813	225.297	1.702	2178	-5	70	0.25	1.189 0.014 2	30.97 0.16 1	32.54 0.18	25 0.3 2.7	2.4	1.20	21.9
N5831	226.030	1.221	1894	-5	70	0.26	1.140 0.010 5	30.38 0.15 1	32.17 0.17	18 0.3 2.1	3.3	1.14	20.3
N5839	226.367	1.635	1420	-2	70	0.23	1.190 0.011 2	30.21 0.30 1	31.77 0.30	32 0.7 1.4	4.4	1.24	19.2
N5845	226.505	1.635	1654	-5	70	0.23	1.124 0.012 3	30.21 0.19 1	32.07 0.21	14 0.6 2.4	3.5	0.83	18.8
N5846	226.622	1.607	1917	-5	70	0.24	1.227 0.007 8	30.59 0.19 1	31.98 0.20	23 0.2 3.3	4.2	1.02	22.0
N5866	226.626	55.763	754	-1	0	0.06	1.121 0.009 4	29.05 0.10 3	30.93 0.12	38 0.6 2.3	5.8	0.87	20.4
N5898	229.555	-24.097	2284	-5	71	0.63	1.169 0.009 5	30.67 0.25 1	32.32 0.26	33 0.4 1.8	2.9	2.12	21.1
N5903	229.651	-24.068	2711	-5	71	0.64	1.142 0.011 4	30.87 0.22 1	32.65 0.23	24 0.3 2.4	1.3	2.28	21.5
I1153	239.265	48.168	803	-2	0	0.08	1.197 0.011 3	29.75 0.19 2	31.28 0.21	15 0.4 2.9	5.2	0.83	18.4
N6017	239.314	5.998	1921	0	0	0.23	1.092 0.011 2	30.37 0.31 1	32.37 0.31	16 0.7 1.4	1.3	1.96	18.5
N6548	271.496	18.587	2088	-2	0	0.35	1.244 0.009 3	30.50 0.20 2	31.81 0.21	34 0.6 2.6	1.9	1.77	21.1
N6673	281.279	-62.297	1128	-4	78	0.46	1.189 0.019 1	28.61 0.20 1	30.18 0.23	29 0.6 1.3	3.2	1.38	18.1
N6703	281.829	45.551	2244	-3	0	0.38	1.164 0.006 9	30.45 0.29 3	32.13 0.29	20 0.5 2.0	1.3	2.02	21.0
N6684	282.240	-65.174	846	-2	0	0.29	1.116 0.015 2	28.82 0.22 1	30.72 0.24	72 0.5 1.1	4.8	1.07	20.1
I4797	284.122	-54.306	2544	-4	279	0.34	1.184 0.018 1	30.66 0.18 1	32.24 0.20	23 0.4 1.8	2.1	1.96	20.6
I4889	296.316	-54.344	2393	-5	77	0.23	1.137 0.016 2	30.54 0.13 1	32.33 0.16	20 0.4 3.0	2.2	1.77	20.7
N6869	300.150	66.217	2603	-2	0	0.79	1.164 0.007 5	30.86 0.21 1	32.53 0.22	20 0.5 2.0	1.4	2.34	20.7
N6851	300.890	-48.284	2914	-5	80	0.20	1.137 0.016 3	30.99 0.19 1	32.79 0.21	20 0.4 3.0	0.7	2.04	20.4
N6861	301.830	-48.370	2687	-3	80	0.23	1.221 0.019 2	30.82 0.35 1	32.24 0.36	32 0.5 1.9	1.2	2.47	21.2
N6909	306.911	-47.026	2600	-4	80	0.16	1.064 0.020 2	30.63 0.12 2	32.75 0.16	19 0.4 3.0	1.9	2.00	19.9
N7029	317.968	-49.283	2645	-5	83	0.16	1.138 0.032 1	31.13 0.46 1	32.92 0.49	32 0.5 1.9	1.4	2.27	20.6
N7041	319.136	-48.364	1697	-3	83	0.17	1.139 0.055 2	30.27 0.18 1	32.05 0.31	37 0.4 1.6	3.2	1.66	20.2
N7049	319.751	-48.564	1977	-2	83	0.24	1.174 0.033 1	30.75 0.15 1	32.38 0.22	55 0.5 2.1	2.8	1.58	21.8
N7097	325.056	-42.540	2184	-5	267	0.09	1.176 0.022 2	30.93 0.18 1	32.55 0.21	29 0.2 2.0	3.7	1.55	20.2
N7144	328.179	-48.254	1722	-5	84	0.09	1.161 0.009 5	30.26 0.10 3	31.95 0.12	33 0.2 1.9	3.1	1.65	20.7
N7145	328.334	-47.882	1673	-5	84	0.09	1.133 0.016 2	30.04 0.19 1	31.85 0.21	25 0.3 2.4	2.5	1.76	20.1
N7173	330.515	-31.974	2225	-4	85	0.11	1.150 0.017 1	30.74 0.16 1	32.48 0.19	21 0.3 2.8	2.8	1.89	19.9
N7168	330.530	-51.742	2563	-5	102	0.10	1.184 0.022 2	31.14 0.21 1	32.72 0.24	29 0.2 2.0	1.8	2.36	20.4
N7180	330.576	-20.547	1164	-2	265	0.14	1.109 0.009 4	29.34 0.25 2	31.26 0.26	23 0.4 1.7	3.7	1.35	17.8
N7185	330.734	-20.471	1523	-3	265	0.14	1.080 0.012 2	29.45 0.36 1	31.51 0.37	30 0.6 1.3	1.5	2.18	18.5
N7196	331.478	-50.120	2813	-5	102	0.09	1.211 0.022 2	31.80 0.28 1	33.27 0.30	31 0.2 1.9	2.5	1.86	21.7
N7192	331.708	-64.316	2764	-4	0	0.15	1.174 0.032 1	31.26 0.28 1	32.89 0.32	27 0.3 2.2	1.0	2.60	21.2
N7200	331.788	-49.996	2702	-4	102	0.08	1.183 0.018 3	31.12 0.31 1	32.71 0.32	16 0.5 1.9	2.6	2.03	19.2
N7280	336.615	16.149	1542	-1	0	0.24	1.105 0.009 3	29.98 0.21 1	31.93 0.22	32 0.7 1.4	2.7	1.67	19.1
N7302	338.100	-14.117	2242	-3	0	0.30	1.126 0.016 3	30.03 0.19 1	31.88 0.21	17 0.6 1.3	1.0	2.33	19.2
N7331	339.272	34.419	492	3	0	0.39	1.120 0.017 1	28.72 0.14 1	30.59 0.17	115 0.8 1.5	9.3	0.36	20.9
N7332	339.352	23.798	853	-2	0	0.16	1.107 0.008 4	29.88 0.19 3	31.81 0.20	27 0.6 1.6	7.5	0.61	20.1
I1459	344.290	-36.460	1350	-5	231	0.07	1.194 0.018 1	30.79 0.26 1	32.33 0.28	54 0.3 2.2	4.1	1.49	22.2
N7457	345.250	30.144	478	-3	0	0.23	1.104 0.009 3	28.66 0.20 3	30.61 0.21	30 0.2 2.6	9.3	0.36	18.8
N7454	345.278	16.390	1637	-5	232	0.34	1.123 0.012 4	30.03 0.29 2	31.89 0.30	23 0.5 1.9	3.5	1.23	19.6
N7507	348.032	-28.541	1240	-5	243	0.21	1.196 0.009 4	30.45 0.15 1	31.99 0.17	35 0.2 1.7	3.9	1.20	21.8
N7619	350.061	8.206	3370	-5	87	0.35	1.229 0.009 3	32.23 0.31 2	33.62 0.31	25 0.4 3.5	2.1	2.46	22.9
I5328	353.321	-45.017	2902	-5	0	0.06	1.173 0.023 2	31.26 0.10 2	32.89 0.15	23 0.3 2.5	1.6	2.67	21.2
N7743	356.090	9.934	1283	-1	0	0.31	1.080 0.009 3	29.53 0.15 1	31.58 0.17	14 0.4 1.6	4.1	1.03	19.6
N7796	359.749	-55.457	3078	-4	0	0.04	1.230 0.022 2	32.11 0.38 1	33.49 0.40	23 0.3 2.5	0.8	2.43	22.1

TABLE 2
UNCERTAIN SBF DATA

Galaxy	RA	Dec	v_{CMB}	T	Grp	A_B	$(V-I)$	\bar{m}_I	$(m-M)$	$\langle r \rangle$	Q	PD	\bar{N}_I
N1331	51.618	-21.356	1173	-5	31	0.13	0	29.73 0.32 1	31.80 0.37	21 0.7 1.4	3.6	1.65	17.6
N1521	62.079	-21.052	4070	-5	0	0.18	1.152 0.029 1	32.41 0.36 1	34.14 0.38	21 0.3 2.8	0.2	2.81	22.1
N1700	74.234	-4.868	3844	-5	100	0.19	1.163 0.011 4	31.54 0.14 1	33.23 0.16	26 0.3 2.2	0.6	2.88	21.7
N3413	162.838	32.768	917	-2	0	0.10	0.733 0.015 1	27.44 0.23 1	31.05 0.24	18 0.5 1.9	4.7	0.78	16.2
N3522	166.669	20.086	1590	-5	0	0.10	0	30.02 0.21 1	32.03 0.28	18 0.5 2.0	3.2	1.30	18.1
N3962	178.666	-13.973	2192	-5	244	0.20	1.145 0.023 1	30.98 0.48 1	32.74 0.49	36 0.4 1.7	0.8	2.85	21.8
N4168	183.069	13.207	2653	-5	0	0.16	1.132 0.015 1	30.63 0.41 1	32.45 0.42	19 0.6 2.3	-0.4	2.31	20.8
N4233	184.277	7.623	2726	-2	150	0.10	1.191 0.015 1	31.09 0.93 1	32.65 0.94	32 0.7 1.4	-0.6	2.43	20.3
N4281	185.090	5.387	3089	-1	150	0.09	1.167 0.015 1	30.28 0.26 1	31.94 0.28	27 0.3 2.6	-0.1	2.22	20.3
N4627	190.499	32.575	1102	-5	248	0.07	0.911 0.015 1	27.04 0.13 1	29.86 0.15	27 0.2 1.6	3.4	1.32	15.4
N4767	193.472	-39.714	3298	-5	58	0.46	1.175 0.028 2	30.95 0.21 1	32.58 0.25	19 0.3 2.2	1.0	2.80	20.8
N5011	198.216	-43.097	3371	-5	62	0.43	1.189 0.027 1	31.54 0.18 1	33.11 0.22	22 0.3 2.7	0.9	2.73	22.0
N5193	202.973	-33.235	3932	-5	64	0.24	1.164 0.034 1	30.99 0.25 2	32.66 0.29	20 0.3 3.0	0.0	2.91	20.6
N5869	227.455	0.470	2314	-2	70	0.23	1.161 0.014 5	30.28 1.22 1	31.98 1.22	8 0.7 1.3	-0.1	2.24	19.7
N6702	281.741	45.707	4600	-5	0	0.47	1.149 0.006 8	31.76 0.23 1	33.51 0.24	13 0.4 2.9	0.4	2.71	21.1
I4943	301.618	-48.374	2799	-5	80	0.22	1.133 0.023 2	30.67 0.15 2	32.48 0.19	15 0.5 1.9	1.4	2.80	19.2
N6868	302.474	-48.379	2742	-5	80	0.24	1.230 0.009 4	30.76 0.24 1	32.14 0.25	26 0.3 2.3	0.3	2.77	21.4
I5269	344.425	-36.017	1846	-2	231	0.07	0	30.15 0.24 1	32.02 0.30	22 0.7 1.4	1.8	2.40	19.1
N7562	348.989	6.688	3231	-5	87	0.45	1.187 0.018 1	32.22 0.83 1	33.79 0.84	32 0.7 1.4	0.2	2.97	22.0

TABLE 3
SBF COLOR DATA

Galaxy	$\langle r \rangle$	\bar{m}_V	\bar{m}_R	\bar{m}_I	$(V-I)$	$\bar{m}_V - \bar{m}_R$	$\bar{m}_V - \bar{m}_I$
N0147		24.51 0.09	23.39 0.09	22.29 0.09	1.030	1.12 0.12	2.22 0.12
N0185		24.38 0.11	23.21 0.09	21.98 0.08	1.023	1.18 0.14	2.40 0.14
N0205	8	23.72 0.17	23.22 0.18	22.26 0.17	0.845	0.50 0.24	1.46 0.24
N0205	16	24.32 0.16	23.53 0.10	22.28 0.08	0.895	0.79 0.19	2.04 0.18
N0205	33	24.60 0.09	23.60 0.09	22.35 0.08	0.965	1.00 0.12	2.25 0.12
N0205	66	24.77 0.08	23.67 0.08	22.43 0.08	0.995	1.10 0.11	2.34 0.11
N0205	132	24.77 0.08	23.67 0.08	22.45 0.08	0.985	1.10 0.11	2.32 0.11
N0221		25.43 0.09	24.20 0.09	22.84 0.09	1.139	1.22 0.12	2.59 0.12
N0224		25.51 0.09	24.53 0.09	22.96 0.09	1.233	0.98 0.12	2.54 0.12
N0404		28.13 0.13	26.99 0.09	25.48 0.09	1.063	1.14 0.16	2.65 0.16

TABLE 4
SBF GROUPS

Group	Example	RA	Dec	v_h	7S#	$(m-M)$	D	N
LocalGroup	N0224	10.0	41.0	-300	282	24.48 0.05	0.79 0.02	2
Cetus	N0636	24.2	-7.8	1800	26	31.97 0.09	24.8 1.1	5
N1023	N1023	37.0	35.0	650	0	30.00 0.11	10.0 0.5	4
Eridanus	N1407	53.0	-21.0	1700	32	32.00 0.08	25.1 1.0	7
Fornax	N1399	54.1	-35.6	1400	31	31.49 0.04	19.9 0.4	26
Dorado	N1549	63.7	-55.7	1300	211	31.34 0.08	18.5 0.7	6
M81	N3031	147.9	69.3	-40	299	28.01 0.12	4.0 0.2	2
LeoIII	N3193	153.9	22.1	1400	45	32.38 0.15	29.9 2.2	2
LeoI	N3379	161.3	12.8	900	57	30.22 0.06	11.1 0.3	5
LeoII	N3607	168.6	18.3	950	48	31.69 0.08	21.8 0.9	5
UMa	N3928	180.0	47.0	900	155	30.84 0.10	14.7 0.8	6
N4125	N4125	181.4	65.5	1300	54	31.82 0.17	23.1 2.0	3
ComaI	N4278	184.4	29.6	1000	55	31.07 0.10	16.4 0.8	4
N4386	N4386	185.6	75.8	1650	98	31.87 0.17	23.6 2.0	3
Virgo	N4486	187.1	12.7	1150	56	31.15 0.03	17.0 0.3	31
ComaII	N4494	187.2	26.1	1350	235	31.14 0.09	16.9 0.8	3
Centaurus	N4696	191.5	-41.0	3000	58	32.64 0.08	33.8 1.4	9
N5011	N5011	197.5	-42.8	3100	62	33.28 0.14	45.3 3.1	2
CenA	N5128	200.0	-39.0	550	226	28.06 0.11	4.1 0.2	2
N5322	N5322	212.5	57.0	2000	254	32.29 0.15	28.7 2.2	4
N5846	N5846	226.0	1.8	1700	70	32.17 0.09	27.1 1.2	5
Telescopium	N6868	301.6	-48.5	2900	80	32.57 0.10	32.7 1.6	5
N7331	N7457	338.7	34.2	800	0	30.60 0.14	13.2 0.9	2